

# FY-2018 FES Joint Research Target

Final Report for the period  
October 1<sup>st</sup>, 2017 through September 30<sup>th</sup>, 2018

Prepared for the US Department of Energy



by the JRT-18 Coordination Committee:

M. Podestà and N. N. Gorelenkov, PPPL

C. S. Collins, General Atomics

W. W. Heidbrink, UC Irvine

Y. Lin, MIT



## Contents

<b>FES Joint Research Target for FY18</b>	2
<b>Executive summary</b>	3
A. Contributors to JRT-18 activities	5
B. Summary of the main achievements during the first three JRT-18 Quarters	6
C. Summary of previous interpretive EP transport analysis	8
1. Analysis of DIII-D discharge #159243	8
2. Analysis of NSTX discharge #141711	11
<b>Main activities during the 4<sup>th</sup> JRT-18 Quarter</b>	14
D. Improvement and validation of modeling tools	16
1. Improved criterion for AE regime prediction	16
2. Development, verification and validation of the RBQ-1D model	17
3. Development, verification and validation of the Kick model	18
4. The ALPHA <i>critical gradient</i> model	21
5. Additional validation of NOVA-K damping rate calculations	22
E. Improvement of diagnostic and analysis tools	29
1. Development and validation of an Imaging Neutral Particle Analyzer on DIII-D	29
2. FIDASIM analysis for experiment/modeling comparison	30
F. Validation of scenario predictions in TRANSP	34
G. Steady-state high q-min scenario for AE studies on DIII-D	38
1. DIII-D discharge #176042	38
2. Predictive EP transport modeling	39
3. Interpretive EP transport modeling	50
H. Interpretation of the JRT-18 results: resolving the RBQ-1D vs. kick discrepancy	51
<b>Recommendations for future experimental and modeling activities</b>	56
<b>Dissemination of the JRT-18 Results</b>	58
<b>Acknowledgements</b>	60
<b>References</b>	61

**FES Joint Research Target for FY18**

*Conduct research to test predictive models of fast ion transport by multiple Alfvén eigenmodes*

Fusion alphas and injected energetic neutral particle beams provide an important source of heating and current drive in advanced tokamak operating scenarios and burning plasma regimes. Alfvén eigenmode instabilities can cause the redistribution or loss of fast ions and driven currents, as well as potentially decreasing fusion performance and leading to localized losses. Measured fast ion fluxes in DIII-D and NSTX-U plasmas with different levels of Alfvén eigenmode activity will be used to determine the threshold for significant fast ion transport, assess mechanisms and models for such transport, and quantify the impact on beam power deposition and current drive. Measurements will be compared with theoretical predictions, including quantitative fluctuation data and fast ion density, in order to validate models and improve understanding of underlying mechanisms. Model predictions will guide the development of attractive operating regimes.

**Milestone for 4<sup>th</sup> Quarter:**

Consolidate results from the analysis of NSTX/NSTX-U and DIII-D data, including results from collaborative experiments from FY-18. Prepare a joint report documenting the progress made toward the JRT goals. Identify open issues and provide guidance for future work based on the JRT results.

### Executive summary

The Fourth Quarter Milestone and the overall JRT goal for FY-18 have been met by completing a detailed assessment of the predictive capabilities of reduced fast ion transport models. The assessment has mainly focused on the effects of Alfvénic instabilities on fast ion transport. Additional activities have extended the assessment to low-frequency MHD instabilities such as kink, fishbones and tearing modes.

- The reduced 'kick' and RBQ-1D fast ion transport models [1][2][3] have been applied to a variety of NSTX/NSTX-U and DIII-D discharges featuring Alfvénic activity and reduction in fast ion confinement. Overall, the models can reproduce experimental observations for properties of the unstable AE spectrum derived from experimental measurements (semi-predictive analysis).
- Predictive capabilities of the models have been pushed to self-consistently determine the expected unstable AE spectrum and associated fast ion transport. Models are successful in reproducing general features of the experiments, such toroidal mode number and frequency range of the dominant instabilities. Predicted fast ion transport levels are typically within  $\pm 10\%$  with respect to the experimental values, as inferred for example from the neutron rate. However, details of the simulations may differ from phase-space resolved measurements (e.g. from FIDA), see below.
- Predictive fast ion transport simulations have been successful in guiding the optimization of tokamak discharges, as demonstrated in DIII-D experiments whose target discharge was pre-designed following the *Predict First* recipe.
- Modeling tools for fast ion transport by instabilities in TRANSP are being extended to account for low-frequency MHD instabilities such as kink modes, fishbones and tearing modes that are occasionally observed in experiments in concomitance with strong Alfvénic activity.
- Results from predictive simulations with the reduced fast ion transport models reveals discrepancies with details of the measured AE spectrum and associated transport. A comprehensive benchmark between the models led to identify the main physics elements that affect simulation results, which are now being considered for further improvements to the models.

- Analysis tools for the interpretation of fast ion diagnostic data have been considerably improved. Previous analyses have been revised, revealing the high sensitivity of the analysis results on diagnostic calibration factors (including fine details of NB injection geometry).
- The detailed comparison between simulation prediction and experimental results has resulted in a comprehensive set of suggestions for future research, including potential improvements to (i) the experimental approach to study fast ion transport by instabilities and to (ii) code improvements to facilitate the comparison with experiments and to improve simulation fidelity.
- Overall, JRT-18 results indicate that reduced fast ion transport models are a valuable tool for the interpretation of present experiments and a very promising avenue to assist experimental planning and scoping activities for new scenarios and future devices.

*Results are provisional and subject to further revisions.*

**A. Contributors to JRT-18 activities***Columbia University:*

- F. Turco

*General Atomics:*

- L. Bardóczi, J. R. Ferron, D. C. Pace, K. Thome, M. A. Van Zeeland, B. S. Viktor, R. E. Waltz

*LLNL:*

- C. Holcomb

*MIT:*

- V. Aslanyan, N. Fil, M. Porkolab

*PPPL:*

- M. D. Boyer, V. Duarte, M. Gorelenkova, B. Grierson, D. Kim, G. J. Kramer, N. Logan, G. Meng, F. M. Poli, Z. Wang, R. B. White

*University of California - Irvine:*

- X. D. Du, D. Lin, D. Liu, L. Stagner, Y. B. Zhu

*University of California - San Diego:*

- E. M. Bass

*University of Wisconsin - Madison*

- G. R. McKee

## B. Summary of the main achievements during the first three JRT-18 Quarters

This Section summarizes progress made during the first three Quarters of the JRT-18 activities. More details can be found in the progress reports for Quarters 1 through 3.

- Candidate reduced models have been identified for the JRT-18 work. The models fall into two main categories: (i) models with some degree of fast ion phase space resolution ('kick' and RBQ-1D models [1][2][3]), and (ii) models based on a "critical density gradient" paradigm (ALPHA/TGLFEP [4][5][6]). (See Sec. D for more details on the different models).
- Analysis of previous NSTX/NSTX-U and DIII-D data was completed, including assessment of the effects of Alfvénic instabilities on Neutral Beam current drive. The analysis was extended to include a comparison between results from the *kick model* in TRANSP with results from a simpler fast ion transport model based on an ad-hoc diffusivity. The comparison reveals the limitations of the ad-hoc model when accurate calculations of fast ion properties are required.
- Analysis of NSTX/NSTX-U and DIII-D discharges indicates a high sensitivity of the simulation results on mode stability properties. Activities on validation of Alfvén Eigenmode stability properties (e.g. damping rates) against available experimental data are ongoing to assist the validation of the reduced models and their interpretation.
- Three JRT-related experiments were executed on DIII-D. A dedicated experiment has confirmed the potential of a new Imaging Neutral Particle Analyzer to provide phase-space resolved information on fast ion transport by instabilities, as required for a quantitative assessment of the performance of fast ion transport models. A second experiment provided a good target for preparatory analysis in view of the main JRT-related experiment. The main experiment of the JRT-18 was executed on DIII-D (March 13th, 2018), providing data on fast ion transport by Alfvénic activity required to test the models during the 3rd and 4th Quarters of FY-2018.
- Initial predictive analysis of DIII-D selected discharges has been completed. The main scenario for this investigation is a steady-state high q-min discharge with strong Alfvénic activity modified through pellet injection. Analysis of Alfvénic modes was performed through the NOVA/NOVA-K codes for the selected DIII-D discharge, which provides the baseline data for RBQ-1D and kick model analysis.

- The tokamak transport code TRANSP has been upgraded with significantly new capabilities to enable simulations with reduced transport models featuring increasing level of fidelity. Based on findings from the JRT-18 activities, plans are being defined for further improvements to include a self-consistent treatment of MHD effects on fast ion transport in time-dependent simulations.

### C. Summary of previous interpretive EP transport analysis

This Section summarizes previous activities on EP transport modeling for NSTX and DIII-D scenarios conducted from FY-15 up to the FY-18 JRT Milestone. For each device, interpretive analysis from a well-diagnosed discharge is discussed to illustrate the achievements of reduced EP transport models when used as analysis tools for actual discharges. Interpretive analysis is typically constrained by far more experimental data than predictive analysis. Thus, results from this Section can be interpreted as representative of the upper limits for what reduced EP transport models can achieve in terms of predictive capabilities. Results from the following two Sections provide a useful comparison for the latest results from predictive use of the reduced EP transport model, which are discussed in Sec. G.

#### 1. Analysis of DIII-D discharge #159243

(Most of the following material is reproduced from Ref. [7]).

DIII-D discharge #159243 has an average injected NB beam power of 6.4MW, resulting in the destabilization of  $\sim 10 - 15$  unstable RSAEs and TAEs (see Fig.1). One of the NB sources is modulated, which enables a conditional averaging of fast-ion signals over a  $\approx 250$  ms time window - from 624 ms to 897 ms - to infer the average fast ion response to NB modulation.

The first step of the analysis is to use magnetic, Motional Stark Effect (MSE) measurements and thermal pressure data to prepare the equilibria that are consistent with MHD spectroscopy.

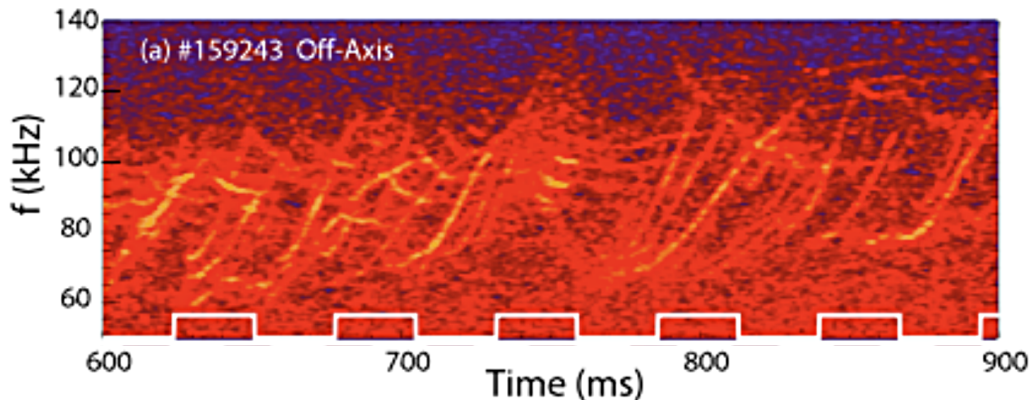


FIG. 1: Spectrum from the cross-power of two CO<sub>2</sub> interferometer chords for DIII-D discharge #159243. The color scale is logarithmic in the amplitude. Waveform for a modulated NB source is shown as a white line. Coherent activity below 50 kHz and above 140 kHz is negligible. (Adapted from Ref. [7]).

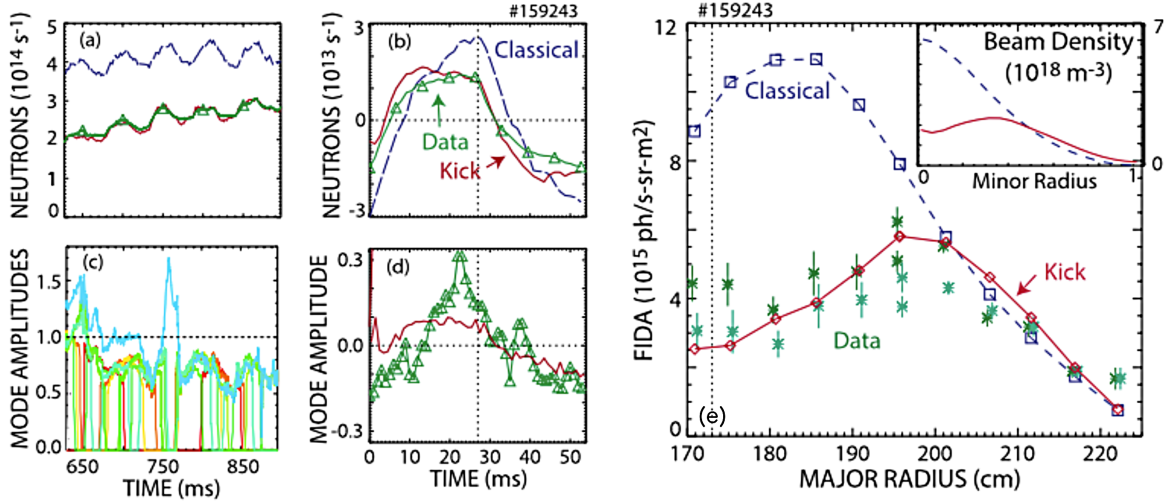


FIG. 2: (a) Comparison of the measured neutron rate (red) with the classical prediction (blue, dashed) and prediction of the kick model (green, solid) as a function of time. (b) Neutron rate response to NB modulation after conditional averaging over 5 cycles of the modulated beam. (c) Evolution of mode amplitudes used in the kick modeling. The dashed horizontal line indicates the approximate value of the measured amplitude at 780 ms. (d) Fractional variation of the measured AE amplitude (green symbols) and of the sum of the modeled amplitudes (solid) after conditional averaging. The vertical dashed lines in panels (b) and (d) show when the modulated beam turns off. (e) Comparison of measured (green asterisks) FIDA brightness profile at 785 ms with simulated profiles. Square symbols indicate the classical prediction. Solid line with diamonds is the prediction from the kick model analysis. The inset shows the total beam-ion density vs. normalized minor radius for the two calculations. The dotted vertical line indicates the location of the magnetic axis. (Adapted from Ref. [7]).

The NOVA code calculates AEs that are matched by frequency, toroidal mode number, and radial structure to electron cyclotron emission (ECE) profiles, as in Ref. [8]. The NOVA mode amplitude is scaled based on the measured amplitude of electron temperature fluctuations,  $\delta T_e/T_e$ . The scaled NOVA modes are used in ORBIT to compute the transport probability matrices for the kick model.

Transport probabilities are inferred assuming a fixed  $q$  profile and constant frequencies and eigenfunctions for the modes. To evolve the mode amplitudes in time, the kick probabilities are multiplied by time-dependent amplitude scaling factors. Figure 2c shows the employed scaling factors for the 9 different modes (or group of modes). These factors are selected to match the measured neutron rate (Fig. 2a), with the RSAE temporal evolution also taken into consideration. To match the neutrons, the utilized mode amplitudes average 77% of the experimentally measured values.

After conditional averaging, the modeled neutron rate is not an exact match to the measured

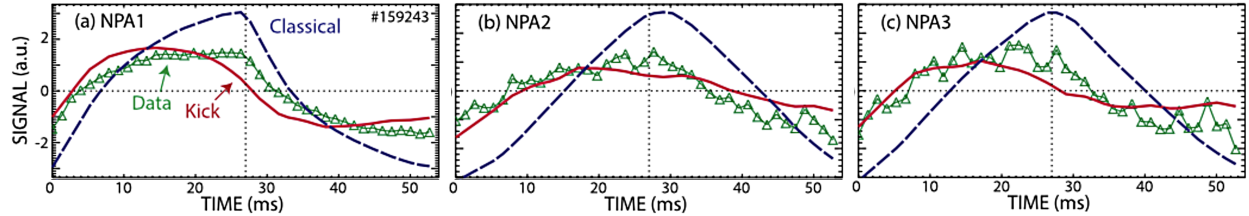


FIG. 3: Comparison of the conditionally averaged measured signal (green triangles) with the classical prediction (dashed line) and with the prediction of the kick model (red, solid) for NPA sightlines that cross the midplane at (a) 183 cm, (b) 165 cm, and (c) 150 cm. Conditional average includes data over 5 cycles between 624 and 897 ms. The vertical dashed lines show when the modulated beam turns off. (Adapted from Ref. [7]).

rate but does follow the general trends, see Fig. 2b. Figure 2d shows an independent check on the modeled amplitude variation. The conditionally-averaged mode scaling factors are close to the measured variation in AE amplitude in the negative portion of the modulation cycle but differ from the measurement in the positive phase.

The output of the kick TRANSP analysis is the fast-ion distribution function  $f$ . The forward-modeling code FIDASIM [9] uses  $f$  to predict FIDA and NPA signals. The calculated fast-ion density profile is slightly hollow (cf. inset of Fig. 2e). Based on the FIDA calibration available at the time of this analysis, this distribution function yields a calculated FIDA profile in good agreement with experiment (Fig. 2e). The central FIDA signal is only 1/3 of the classical prediction. Physically, the hollow profile may be associated with the finite orbit size of the fast ions. Fast ions on orbits that produce appreciable FIDA signal can traverse the magnetic axis and the  $q_{min}$  location, so RSAE-induced transport can easily affect the central fast-ion density. It should be noted that FIDA signals were more recently re-analyzed based on updated NB geometry in the FIDASIM code. The new analysis, discussed in Sec. E 2, suggests a less favorable comparison between kick model results and FIDA measurements.

The predicted NPA signals are close to the experimental measurements. Figure 3 compares the conditionally averaged measurements for the three NPA sightlines with the kick predictions after processing by FIDASIM. Both the magnitude and time evolution are as close to the experimental values as the agreement with the neutron signal that was used to infer the mode amplitudes. The NPA channels are sensitive to the trapped-particle population, while the neutron diagnostic is sensitive to all pitch angles. The good agreement of the kick prediction with the NPA signals suggests that the interaction of AEs with trapped particles is accurately treated by the modeling.

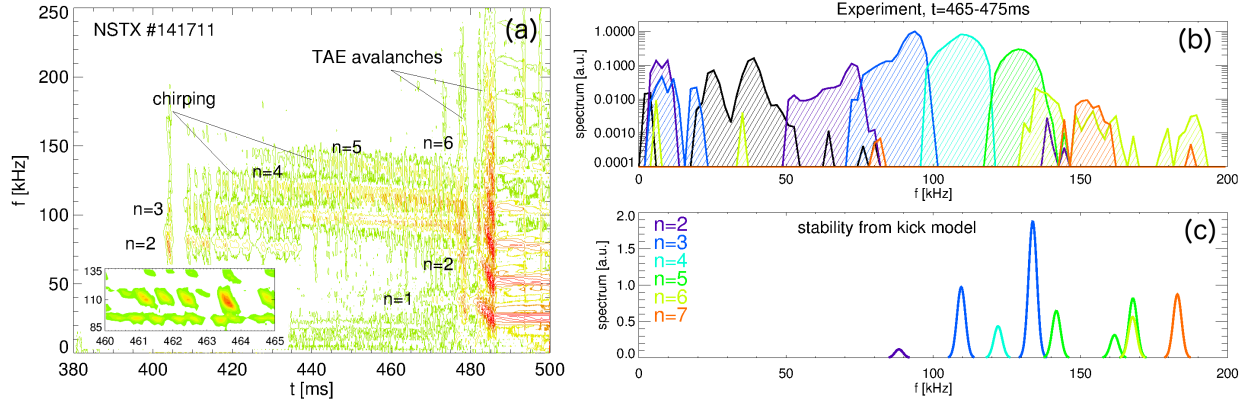


FIG. 4: (a) Measured spectrum of magnetic fluctuations from a Mirnov coil for NSTX discharge #141711. Toroidal mode numbers are indicated by labels for each mode. The inset shows a detail of the evolution of bursting/chirping modes. Mode amplitude in the figure is increasing for colors from green to red. (b) Mode number spectrum from the experiment and (c) comparison with stability results from the kick model. Colors refer to different toroidal mode numbers according to the labels in panel (c). (Adapted from Ref. [2]).

For this discharge, the RBQ-1D model was also benchmarked against kick model analysis, resulting in an overall agreement between the two models. A summary of the benchmark activities was reported in the First Quarter Report of the JRT-18.

## 2. Analysis of NSTX discharge #141711

(Most of the following material is reproduced from Ref. [2]).

The NSTX discharge #141711 is selected to illustrate the use of the kick model for interpretive analysis. Toroidal field is  $\sim 0.5$  T, with density  $\approx 4 \times 10^{19} \text{ m}^{-3}$  during the time of interest,  $380 \leq t \leq 520$  ms. Electron and ion temperatures are  $T_{e,i} \sim 1$  keV and central plasma rotation is 25 – 40 kHz. The injected NB power is  $P_{NB} = 2$  MW from a single NB source with injection energy of 90 keV. Toroidal Alfvén Eigenmodes are destabilized during the time of interest with frequency 50 – 200 kHz and toroidal mode number  $n = 2 - 6$  (Fig. 4a-b). Modes exhibit a weak bursting/chirping nature, with relative frequency variations  $\lesssim 10\%$ . Notably, the chirping regime for this scenario is consistent with predictions from the recently developed criterion for the occurrence of chirping AEs, cf. Refs. [10][11].

The initial NOVA analysis, from which about 50 candidate eigenmodes are extracted, is performed based on profiles at  $t = 470$  ms. The next step consists in running TRANSP with the selected modes to infer their linear stability. Of the original eigenmodes, only twelve modes are

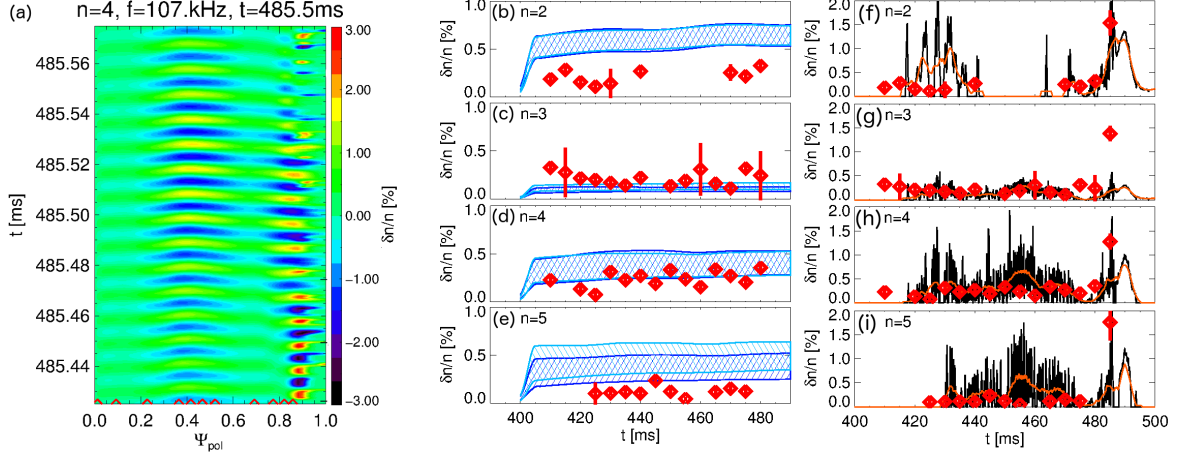


FIG. 5: (a) Example of relative density perturbation,  $\delta n/n$ , inferred from reflectometers measurements for a  $n = 4$  TAE mode. Symbols on the x-axis indicate the measurements position. Maximum of the fluctuation is computed for  $0 \leq \Psi \leq 0.7$  ( $\Psi$ : normalized poloidal flux), removing edge regions for which the inferred  $\delta n/n$  is unreliable. (b)(e) Comparison between measured (symbols) and predicted (hashed regions) density fluctuations. Kick model results are shown from two set of unstable modes with light/dark blue. For each set, amplitude is computed assuming damping rates from NOVA-K and for a constant value  $\gamma_{damp} = 1\%$ . (f-i) Same as in panels (b-e) with mode amplitudes obtained by iterating TRANSP runs to achieve a good match between simulated and measured neutron rate. The solid red line represents a running average of the bursting amplitudes. (Adapted from Ref. [2]).

found unstable with net growth rates  $\gamma/\omega \lesssim 2\%$ . The predicted unstable spectrum is limited to  $n = 2 - 7$  in the frequency range 70 – 180 kHz (Fig. 4c), whereas  $n = 1, 8$  modes are stable.

As an initial test of using the kick model for predictive analysis, the linearly unstable modes are divided into two sets to investigate their amplitude saturation level. The first set includes the most unstable modes with  $n = 2 - 7$ . In the second set, the second most unstable modes are used for those  $n$ 's that result in more than one unstable mode (this second set of modes is a closer match to the experimental spectrum). For both sets of unstable modes the kick model predicts a reduction in neutron rate of 5 – 10% with respect to classical TRANSP simulations, depending on the damping rate used to infer the saturated mode amplitudes (values from NOVA versus constant  $\gamma_{damp}/\omega = 1\%$ ). These values are consistent with the measured neutron rate deficit, which increases from 0 as the NB injection starts up to  $\approx 10\%$  in the later part of the discharge. (A larger drop in neutron rate of  $\approx 30\%$  around  $t = 485$  ms, corresponding to the spike in amplitude fluctuations shown in Figs. 5f-i, is caused by a TAE *avalanche* and is not considered in this analysis).

The results obtained from the semi-predictive kick model analysis described above are then expanded to include information that is available from the real experiment. This is done to (i)

perform an initial assessment of the validity of the predictions against the actual experiment and (ii) to illustrate the additional insight that can be gathered using the model in interpretive mode. For instance, weak  $n = 1$  activity is occasionally detected in the magnetic fluctuation spectrum (Fig. 4a). This coincides with times at which multiple modes have significant amplitude. Previous work has indicated that the observed  $n = 1$  activity is the result of three-wave coupling between pairs of TAEs with adjacent toroidal mode numbers and  $n = 1$  kink-like activity [12][13]. Kink modes are not included in the predictive analysis, but can be introduced for the interpretive use of the kick model.

The additional information from the experiment is then used to further tune the kick model parameters to achieve a better match with the experiment. For example, experimental mode amplitudes are not quasi-stationary, as assumed for the predictive analysis, but feature repetitive bursts as time evolves. The (relative) amplitude evolution for each toroidal mode number is therefore inferred from Mirnov coils measurements for the interpretive analysis. As a second step, the information on three-wave coupling processes present in the experiment is used to mimic the presence of a time-dependent  $n = 1$  kink mode. Finally, mode amplitudes are rescaled until a good match between simulated and measured neutron rate is achieved.

The comparison between kick model results and the actual experiment is shown in Fig. 5. Experimentally, an array of reflectometers [14][15] is used to measure the local density fluctuations,  $\delta n/n$ . Analysis of reflectometer data follows the method first proposed in [13] to infer the density perturbation evolution over the short time-scale of a TAE burst. An example is shown in Fig. 5a for a  $n = 4$  TAE. For the comparison with the kick model results, analysis of reflectometer data is performed every 5 ms from 410 ms to 490 ms and  $\delta n/n$  is inferred for each mode with  $n = 2 - 5$ . For the kick model,  $\delta n/n$  is obtained by rescaling the values computed by NOVA to take into account the actual mode amplitudes used for the simulation. Values of  $\delta n/n$  from the kick model analysis and the experiment are compared in Figs. 5b-e (predictive) and in Figs. 5f-i (interpretive).

For predictive analysis, the agreement with the experiment is usually within a factor of two. A general trend is that the kick model tends to over-predict the density perturbation, suggesting that the predicted mode amplitudes are larger than the actual ones. For the interpretive analysis, the inferred values of  $\delta n/n$  are also in qualitative agreement with the measured perturbations, although some differences are sometimes observed in the time evolution. In general, however, discrepancies remain within a factor  $\lesssim 2$  or better over most of the simulation time range, which can be considered a satisfactory result for the reduced kick model.

## Main activities during the 4<sup>th</sup> JRT-18 Quarter

The main JRT goal during the last Quarter was to test reduced EP transport models that are based on different physics assumptions in order to identify their potential for predictive simulations. The models included in this exercise differ for level of complexity, physics fidelity and computational cost [16], as summarized in Fig. 6. Compared to previous work (cf. Sec. C), simulations that aim at predicting the time-dependent behavior of the instabilities themselves - in addition to the fast ion transport resulting from those instabilities - are certainly a major challenge. The accomplishments discussed in the remainder of this Report provide a first assessment of the present status for EP-driven instabilities and associated fast ion transport.

Activities in the Fourth JRT-18 Quarter have a solid basis in work carried on during FY-18. The main achievements are summarized in Sec. B, which is based on the previous JRT-18 Quarterly Reports.

The common ground for most activities is the use of the tokamak transport code TRANSP [17][18][19] and its fast ion module NUBEAM [20]. TRANSP provides a comprehensive platform for integrated, time-dependent tokamak simulations that are not restricted to energetic particle physics but encompass most aspects of tokamak physics such as equilibrium evolution and thermal plasma transport. The NUBEAM module in TRANSP is used to include (neo-)classical fast ion physics, e.g. collisional scattering and slowing down of fast ions from NB injection and atomic

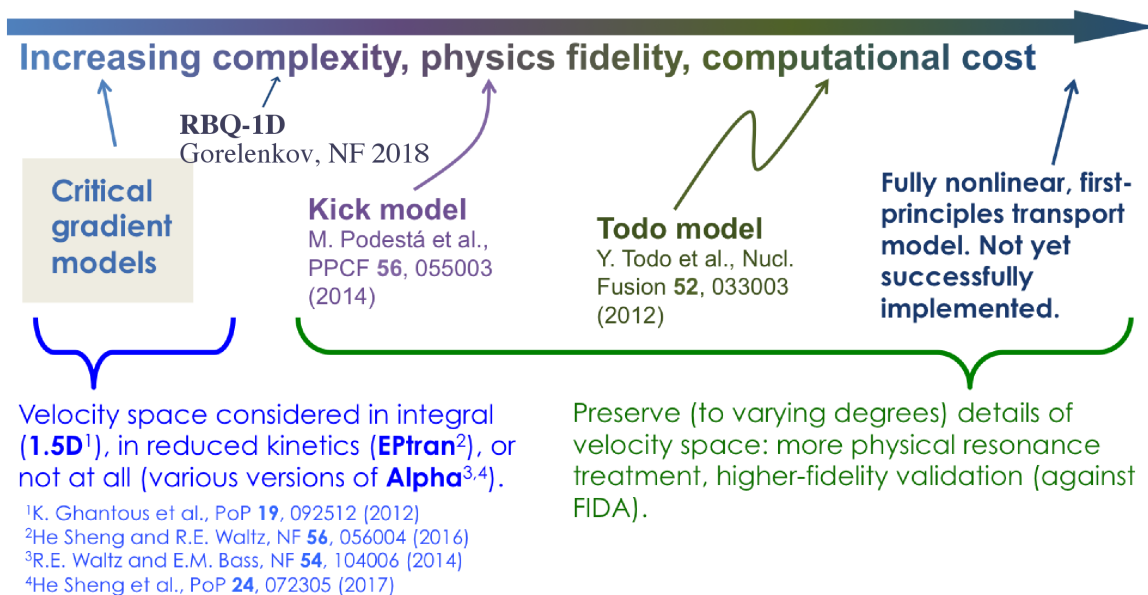


FIG. 6: Schematic of the EP transport model approaches, highlighting the hierarchy from reduced models to 'first-principles' codes. (Adapted from Ref. [16]).

physics processes such as ionization and charge-exchange reactions with background neutrals.

Recent updates to TRANSP/NUBEAM have enabled the inclusion of fast ion transport by instabilities, with inputs produced by either kick or RBQ-1D models. At the same time, other modeling and analysis tools were improved to support JRT-18 activities. The following Sections provide a summary of the main developments achieved during the last Quarter of FY-18.

## D. Improvement and validation of modeling tools

### 1. Improved criterion for AE regime prediction

Considerable progress has been made in the development of an improved criterion to predict the specific regime of unstable AEs based on the characteristic of the background thermal plasma [10]. More specifically, AEs are usually observed in two different regimes characterized by either constant mode frequency and slowly varying amplitude or bursting amplitude with rapid ( $\sim 1$  ms time scale) frequency variations (or chirps). Each regime can lead to substantially different effects on the EP population, from weak redistribution to convective, explosive transport. The improved criterion builds upon previous theory of wave-particle interaction near marginal stability by extending the treatment to realistic mode structures and values of EP scattering (e.g. by thermal plasma fluctuations).

Figure 7 shows an example for a NSTX discharge with unstable TAEs transitioning in time from quasi-stationary to bursting/chirping [11]. The GTS code is used to compute thermal plasma fluctuations, which provide an estimate for the enhanced EP scattering rates. The criterion successfully recovers the observed AE regime transition as time evolves. Similar validation work on DIII-D plasmas [10] gives confidence in the predictions, which have then being applied to ITER scenarios. The criterion suggests that ITER plasmas may be prone to bursting/chirping AEs.

Work is ongoing to compare results from the improved AE chirping criterion to numerical modeling of the formation of EP phase-space structures (so-called *holes* and *clumps*) through wave-particle interaction, which is postulated to be at the origin of the emergence of the AE

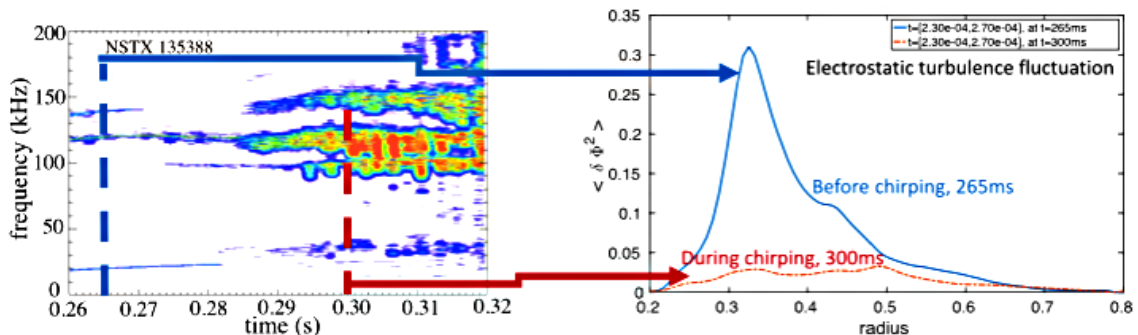


FIG. 7: Left: spectrum of magnetic fluctuations in the TAE range of frequency showing the transition of modes with quasi-stationary frequency to bursting/chirping modes after  $t$  290ms. Right: radial profile of electrostatic turbulence fluctuations at two times from the GTS code. (Adapted from [10]).

chirping regime [21]. Knowing the expected AE regime is crucial to assess the validity of different EP transport models. For instance, the effects of AE in the bursting/chirping regime may not be accurately reproduced by quasilinear theory.

## *2. Development, verification and validation of the RBQ-1D model*

When the dominant mechanism for fast ion transport can be approximated as a diffusive process, quasilinear (QL) theory [22][23] provides a promising reduced approach, which offers the advantage of a simplified and less computationally demanding framework than modeling tools based on first-principles. Starting from previous work on QL theory [24], the Resonance Broadened Quasilinear model RBQ-1D was developed over the last few years to address the particle interaction with both isolated and overlapping Alfvénic modes. This is done by using the same structure of QL equations for fast ion distribution function, but with the zero-width resonances broadened along the relevant path of resonant particles to produce a resonance line broadened diffusion [25].

During FY-18, the implementation of the RBQ-1D model as post-processor for the NOVA-K code was concluded [3]. The diffusive solver in the model has been extensively verified against analytic theory solutions, as reported in the 2nd Quarter Report of the JRT-18. Furthermore, the ability to compute relaxation of the fast ion distribution function under the effects of several modes growing simultaneously was implemented during the 3rd Quarter.

Further progress in RBQ-1D development was achieved during the fourth quarter of the JRT-18. Several key elements of the quasi-linear approach developed earlier for a model problem relevant for a fusion plasma [24] were revisited. One particular aspect is the resonant ion dynamics near the resonance with the Alfvénic eigenmode [26]. Analysis through the ORBIT code has recently demonstrated [27][28] that the pendulum approximation for the bounce frequency,  $\omega_b$ , dependence on the amplitude works well for small amplitudes (i.e. near marginal stability), but needs to be modified for larger amplitudes. Because the RBQ-1D formulation is based on the realistic structure of the unstable mode [3] and on the resonance frequency formalism to measure the wave particle interaction [24], the way the resonant frequency is used in simulations is critical for the broadened resonance approach. The latter is computed using the prescriptions given by the Hamiltonian dynamics of a resonant ion precession within a resonant island [28]. The amplitude is a function of the poloidal flux dependence on the action angle  $Q$ , i.e.  $\psi(Q)$ , which parameterizes the orbit.

Even with the pendulum-like dependence of the bounce frequency over the local amplitude value,  $\omega_b \propto \sqrt{A}$ , asymmetry can be found because of the  $\psi = \psi(Q)$  dependence. The approach

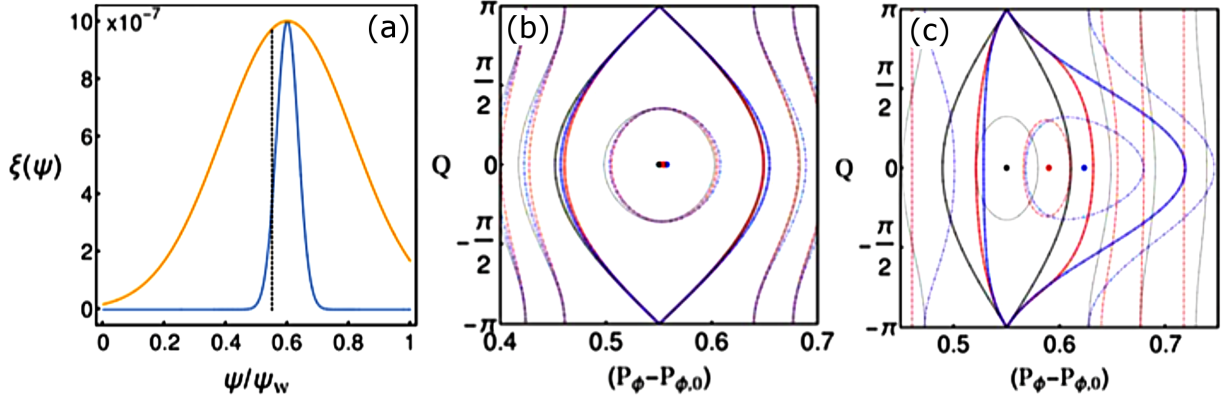


FIG. 8: (a) Gaussian mode structures with the widths  $0.3\psi_w$  and  $0.05\psi_w$ , where  $\psi_w$  is the poloidal magnetic flux at the wall used in ORBIT simulations. (b) and (c) show kinetic Poincar plots for pendulum Hamiltonian framework (black), the first-order Taylor-expanded Hamiltonian around the central action value (blue) and the exact Hamiltonian that accounts for the local values of the mode structure (red). Panel (b) refers to the broad mode structure shown in (a), whereas (c) corresponds to the narrow mode structure. The resonance occurs at  $P_{\phi,0} = 0.65$ . The absolute peak amplitude of the mode is chosen arbitrarily for illustration, so that the absolute broadening width in  $P_\phi$  has no particular meaning. The center of the island is chosen to coincide with a steep variation in mode structure, thereby exacerbating the island asymmetry with respect to its elliptic O-point, represented by the dots in different colors. (Adapted from Ref. [26]).

proposed in Ref. [26] accounts for the next-order correction, due to the derivative (next-order Taylor expansion) of mode amplitude with respect to the action variable but all quantities are evaluated at the center of the island.

### 3. Development, verification and validation of the Kick model

The status of the reduced 'kick' fast ion transport model in TRANSP before FY-18 was summarized in Ref. [2], which discussed the initial use of the model for *predictive* simulations of scenarios with unstable Alfvén Eigenmodes (AEs).

During FY-18, further developments of the kick model have been achieved in three main areas, namely (i) a more comprehensive assessment of the model's predictive capabilities for AEs, (ii) the extension of the model to include effects on fast ion transport from other types of instabilities in TRANSP, and (iii) improvements to the software used to compute the kick model inputs used in NUBEAM/TRANSP.

The ability and main limitations of the kick model to predict the main AE features observed experimentally is discussed in Ref. [29]. Target NSTX and NSTX-U discharges are analyzed in

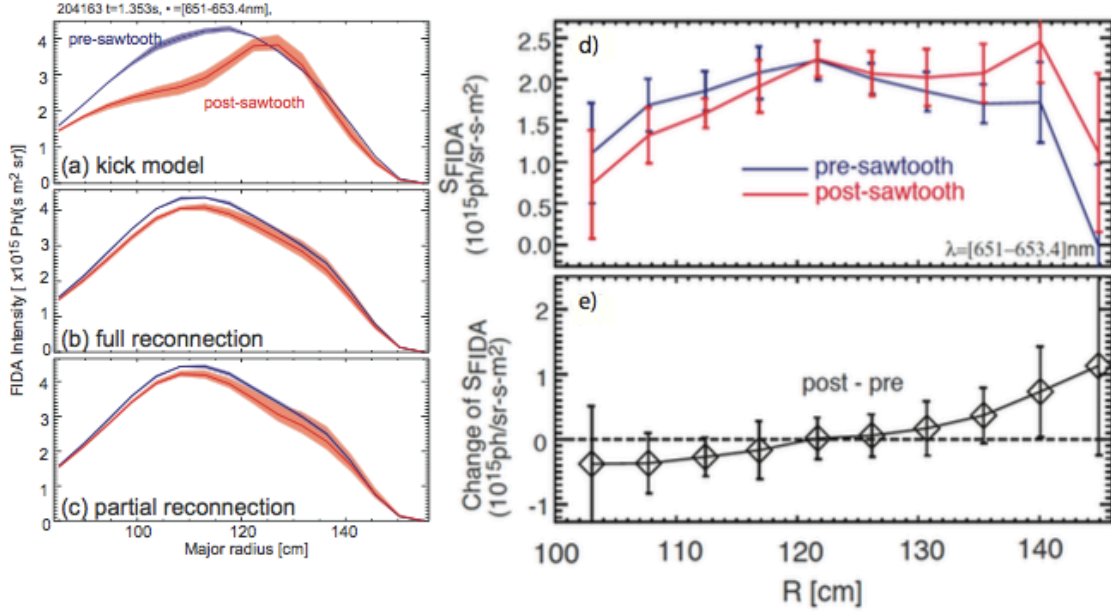


FIG. 9: The distributions of fast ion from FIDA simulation (t-FIDA) using (a) kick model, (b) full reconnection and (c) partial reconnection. All profiles are averaged over three time steps (1, 3, and 5 ms) before and after a crash. The experimental measurement from FIDA signal is shown in (d) and (e). Full/partial reconnection models cannot reproduce the increase in FIDA signal due to a sawtooth crash outside the  $q = 1$  surface ( $R \approx 125$  cm). Kick model simulations show a modification of the fast ion distribution that is qualitatively consistent with the experimental FIDA data. (Adapted from Ref. [30]).

terms of linear stability of AEs and of the effects of AEs on fast ion confinement once the modes reach saturation. Overall, the model can reproduce general features of the measured AE spectrum such as toroidal and frequency spectra. Based on the available measurements of AE radial structure and amplitude, the model can also recover the time-averaged saturation amplitude within a factor  $\approx 2$ . Modeled fast ion transport, as quantified by the deficit in the neutron rate with respect to 'classical' TRANSP simulation, agrees with the measurements well within typical experimental uncertainties of  $\pm 10\%$ .

The extension of the kick model to low-frequency MHD instabilities has made good progress for tearing modes, kink-like modes (kinks, fishbones) and sawteeth. (In this case, the model has been mostly used in *interpretive* analysis with inputs from the actual experiments. Prospects for *predictive* analysis are discussed below). The motivation is to extend the assessment of predictive modeling capabilities to a broader class of scenarios than initially planned for the JRT-18 Milestone, since in general Alfvénic instabilities can coexist with other MHD instabilities.

Initial results on the analysis of DIII-D scenarios with large 2/1 NTMs were reported at the

IAEA Technical Meeting on Energetic Particles (Princeton, NJ) held in Sept. 2017 [31]. Further progress during the JRT-18 period resulted in several presentations [32][33] and publications [34][35]. Results from DIII-D indicate that the kick model can reproduce experimental measurements under a variety of conditions, using measured NTM amplitudes as input.

Progress was also made in testing the kick model for kink, fishbone and sawtooth instabilities [36][37][38], with an initial comparison between modeling and experimental results based on NSTX and NSTX-U plasmas. Compared to the analysis with AEs only, the numerical analysis that provides the input for NUBEAM/TRANSP is generally simplified by the smaller number of active modes and associated resonances. However, no procedure has been developed yet to infer the mode structure from numerical codes and only analytical approximations for the radial structure have been used during FY18. Results obtained during FY18 indicate that simulations based on the kick model to describe enhanced fast ion transport can provide improved agreement with experimental data from fast ion diagnostics such as FIDA for sawtooth scenarios [30][37][38], see Fig. 9.

As the use of the kick model is increasing, an optimized version of the ORBIT code [39] has been developed in FY18. The new version enables multi-processor ORBIT simulations, thus reducing considerably the computing time required to generate the kick model input for NUBEAM/TRANSP. Other features have been introduced to optimize the grids in fast ion variables, over which the input for NUBEAM is defined, at run-time for each specific case. As an example, the new version of ORBIT reduces the time to compute a kick model input for an Alfvénic mode from several hours to less than an hour. The time can be further reduced to only a few minutes for modes with a simple harmonic composition such as kinks and NTMs. Other features are being implemented to enable a direct comparison with other codes (e.g. RBQ-1D). One of the most important of them is the possibility of introducing finite Larmor radius (FLR) corrections to the perturbed fields sampled by particles during their orbiting. At present, this is done by sampling the perturbation radially over a range defined by each particle's Larmor radius, whereas variations along the poloidal direction are neglected. This approximation is expected to break down for higher- $n$  modes, for which the dominant poloidal harmonics have increasingly large  $m$  number ( $n$  and  $m$  being the toroidal and poloidal mode numbers, respectively). Further improvements of the FLR corrections to the guiding-center ORBIT code are being considered, although their use is expected to increase the computing time by (at least) a factor of 2 – 5.

#### 4. The ALPHA critical gradient model

A third reduced EP transport model that has been tested as part of the JRT-18 activities is the ALPHA model [4][5][6]. The model is based on a *critical gradient* paradigm for the EP density, that is the EP profile is assumed to be locally restored by instabilities to a marginally stable profile once a threshold value in the local gradient is exceeded.

Contrary to the RBQ-1D and kick models, it is postulated that the effective EP diffusivity is independent of energy and pitch and that the EP energy transport flux,  $Q_{EP}$ , is purely convective with  $Q_{EP} = (3/2)T_{EP}\Gamma_{EP}$  (here  $\Gamma_{EP}$  is the EP particle flux and  $T_{EP}$  and equivalent EP temperature).

The local critical gradient is determined from the most unstable local eigenmode growth rates, which are computed with the highly parallelized gyro-Landau solver TGLFEP [6] using a Maxwellian EP distribution and the experimental slowing down EP density profile. (Alternatively, the gyrokinetic initial-value solver GYRO [40] can replace TGLFEP to compute the AE growth rates, but the process is more operationally cumbersome and computationally expensive).

For the comparison with other reduced EP transport models, the ALPHA model provides two main outputs: (i) relaxed EP radial density (or pressure) profile; (ii) radially-dependent EP diffusivity coefficient. Under the assumptions of stationary discharges, the EP density/pressure profiles can be directly compared with results from TRANSP simulations with enhanced EP transport included through either RBQ-1D or kick model. As an alternative, the radial EP diffusivity coefficient can be used as input for TRANSP/NUBEAM to evolve the fast ion profiles in a time dependent simulation.

### 5. *Additional validation of NOVA-K damping rate calculations*

The completed JRT-18 research shows that the fast ion transport predictions are very sensitive to the damping rate calculations through the NOVA-K code. Part of the JRT-18 activities have therefore focused on the assessment of the accuracy of damping rate calculations, extending the study to RF-heated plasmas in addition to the common NB-heated discharges from NSTX/NSTX-U and DIII-D.

The GTC code [41] has been set up to compare the damping rates from NOVA/NOVA-K with Alcator C-Mod and JET plasmas in which the damping rate was measured by an active MHD antenna [42]. Target C-Mod discharges were previously studied in depth with NOVA-K [43][44]. More recent work from JET is discussed in Ref. [45].

The work was suspended during FY-18 before conclusive results were obtained because of a personnel departure from the field and it has only recently been resumed by a new postdoc. Initial studies will focus on the study of stable TAEs excited in Ohmic plasmas on Alcator C-Mod. The shot #1050615011 from which a clear resonance has been observed with the active MHD antenna by sweeping up and down through the center of the TAE gap frequency [44] will be studied with GTC. The aim of this work is to use a synthetic antenna developed in GTC to probe the modes damping rates as well as the frequency and to compared them to the measurements made by the active MHD antenna in this shot [43]. This method will also be applied to other Alcator C-Mod plasma shots and compared to NOVA-K results. Secondly, by using GTC, individual damping mechanisms for TAE modes will be identified and quantified thanks to kinetic and non-perturbative models which enable to get more physics insights compared to ideal MHD solvers. To do so, the different physics models available in GTC will be applied in conjunction with the synthetic antenna for direct comparisons of damping rates.

In addition to the ongoing work with GTC, the following paragraphs report on another approach aiming at tackling the damping rate calculation assessment based on NOVA-K simulation on C-Mod experimental data. Near the end of the last Alcator C-Mod campaign, the 3-ion ICRF heating scheme was successfully demonstrated [46]. In the experiment, we have nearly equal amount of D and H plus a trace amount of  $^3\text{He}$  (<1-2%). In addition to typical indicators for ICRF heating, the occurrence of TAEs in some of the 3-ion ICRF heated plasmas was treated as a definite signature of the existence of energetic  $^3\text{He}$  ions produced by direct RF power deposition.

C-Mod results raised the following questions:

- Will NOVA-K predict the occurrence of the TAE mode in these plasmas?

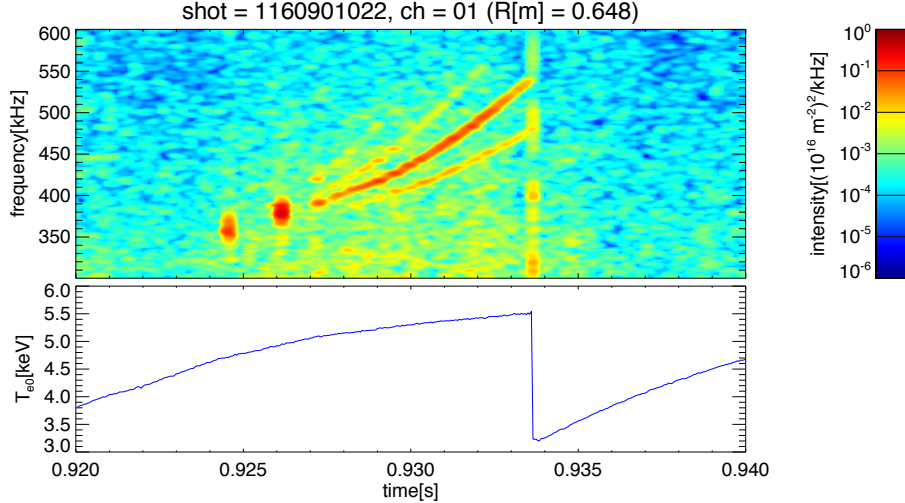


FIG. 10: TAE mode observed in 3-ion ICRF heating experiment (shot 1160901022) on Alcator C-Mod. Top: Spectra from PCI density fluctuations vs. frequency and time; Bottom: Time trace of  $T_{e0}$ .

- What can we tell about the most likely fast ion distribution from the occurrence of TAEs?
- Can NOVA-K give a self-consistent calculation on the driving term and damping term given the experimental observation?

After setting up the most recent NOVA-K version for C-Mod RF-heated plasmas, a number of NOVA-K runs have been carried out. NOVA-K has indeed found modes consistent with the experimental observations, and its prediction of fast particle equivalent temperature,  $T_H$ , based on the mode drive from ICRF fast ion tails seems reasonable. However, the critical fast ion  $\beta_{crit}$  required to excite the mode is larger than what is plausible considering the available experimental constraints. This result indicates that the damping term from NOVA-K may be too high for these plasmas.

#### *Experimental observation and NOVA-K study*

Figure 10 shows one of the two discharges that have been analyzed for TAEs. A mode appears in the fluctuation spectra of the Phase Contrast Imaging (PCI) from  $t = 925$  ms to 934 ms in the frequency range of 350 kHz to 550 kHz. PCI measures the vertical chord averaged density fluctuations. The toroidal mode number of this mode  $n = 2$  as determined from the magnetic coil signals.

NOVA-K runs are set up using experimental data at  $t = 930$  ms. Main plasma parameters are  $T_{e0} = 5.3$  keV,  $n_{e0} = 2.4 \times 10^{20} \text{ m}^{-3}$ ,  $B_{t0} = 7.82$  T,  $I_p = 1.2$  MA, and  $q_{95} = 4.2$ .  $P_{RF} = 4$  MW at

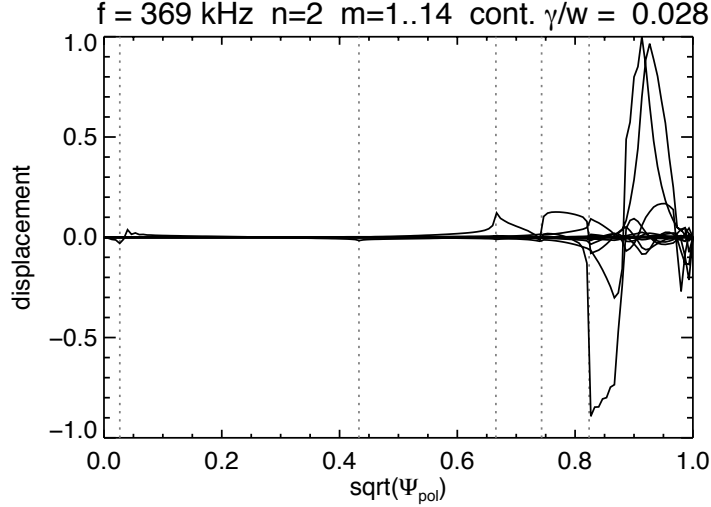


FIG. 11: Displacement  $\xi$  vs. flux surface function  $\sqrt{\Psi_{pol}}$  of the mode at  $f = 369$  KHz from NOVA-K calculation. Input parameters are from  $t = 930$  ms of the plasma shown in Fig. 10.

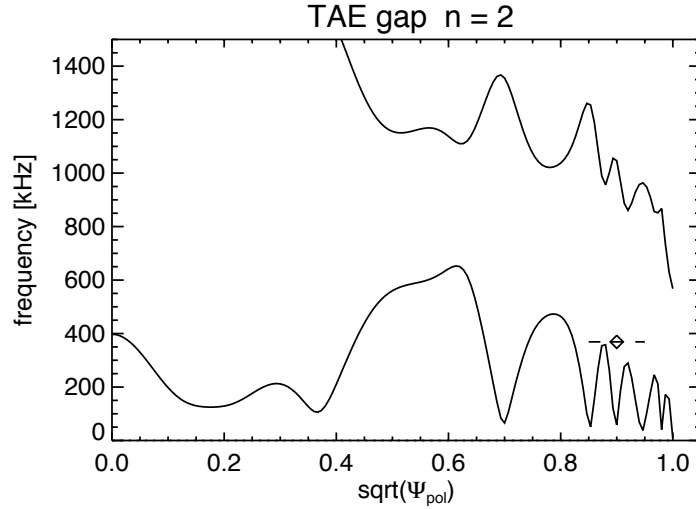


FIG. 12: TAE continuum from NOVA-K. The mode location is shown as the diamond.

this time slice.

NOVA-K indeed finds a mode with  $n = 2$  and  $f = 369$  kHz, very close to that observed in experiment. As shown in Fig. 11 and Fig. 12, the mode is located at the TAE gap just above the lower continuum centered at  $r/a \sim 0.85$ .

To excite TAE, the driving term from the energetic particles (hot ions) must exceed the total damping term. Since the driving term is proportional to the hot ion  $\beta_H$ , there is a critical hot ion  $\beta_{crit}$  that the TAE would be triggered only when  $\beta_H > \beta_{crit}$ . In the experiment, TAEs are not always present and only occur at the time when the heating is supposedly strongest. As a result,

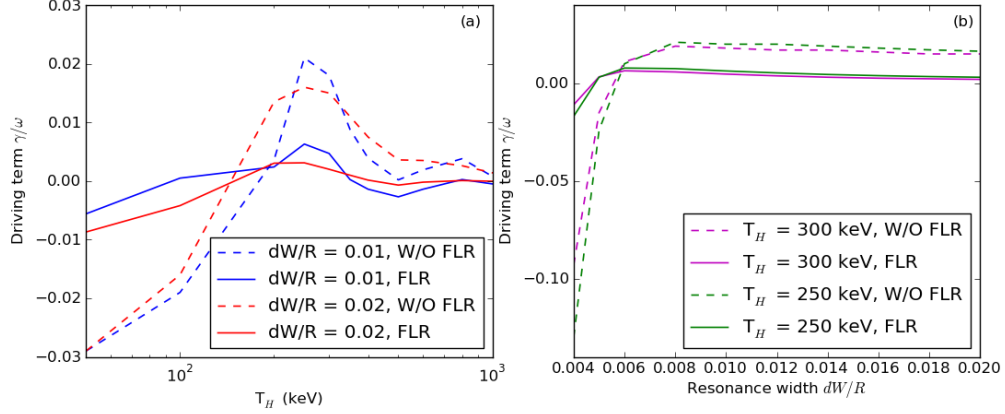


FIG. 13:  $T_H$  and  $dW_{res}$  scan for the driving term. (a)  $\gamma_{drive}/\omega$  vs.  $T_H$  at  $dW_{res}/R = 0.01$  and  $0.02$ , both with FLR and without FLR. (b)  $\gamma_{drive}/\omega$  vs.  $dW_{res}/R$  at  $T_H = 250$  keV and  $300$  keV, both with FLR and without FLR.

they probably occur when the driving term is just above the damping term for TAE stability. The driving term depends on the particle energy and distribution in the velocity space distribution and in the real space.  $^3\text{He}$  ion energy and distribution functions can be estimated using a RF code, like CQL3D. However, in lack of direct experimental measurement, the result of such calculation would be highly uncertain. Here the default form of the fast particle distribution function in NOVA-K is used and parameters are varied to find the distribution that would produce the largest drive at a fixed fast ion  $\beta$ . Because from the experimental observation the fast ion distribution is expected to be near the optimal form for TAE instability, the numerical search looks for the particle distribution that requires the lowest  $\beta_{crit}$  to make the mode unstable.

The default fast particle distribution has the following form in velocity space:

$$f \propto \exp\left(-\frac{E}{T_H} - \left(p - \frac{R_{res}}{R_{axis}}\right)^2 / \left(\frac{dW_{res}}{R_{axis}}\right)^2\right) \quad (1)$$

where  $E = mv^2/2$ ,  $T_H$  is the fast ion temperature,  $p = \mu B_{axis}/E$  is a pitch angle parameter.  $\mu$  is the magnetic moment,  $\mu = mv_{\perp}^2/2B$ .  $R_{res}$  is the  $^3\text{He}$  resonance layer location in major radius and for this experiment,  $R_{res} \simeq R_{axis}$ . The fast ions are assumed to have perpendicular velocity at their banana orbit tips over a small width  $dW_{res}$  about  $R_{res}$ . In real space,  $\beta_H$  is also assumed to have a peak and scale length parameter.

In Fig. 13-(a), the driving term is plotted vs.  $T_H$  at two  $dW_{res}/R$  values and in Fig. 13-(b), the driving term is plotted vs.  $dW_{res}/R$  at two  $T_H$  values. In the simulation,  $\beta_{H0} = 0.01$  and peaks at  $R_{axis}$ . The largest drive is at  $T_H \sim 250 - 300$  keV and for pitch angle width parameter

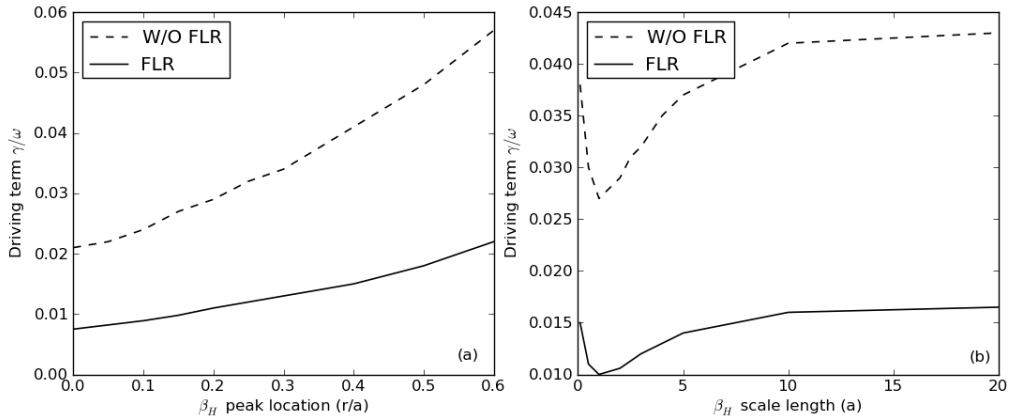


FIG. 14:  $\beta_H$  peak location and scale length scan for the driving term. (a)  $\gamma_{drive}/\omega$  vs.  $\beta_H$  peak location both with FLR and without FLR. (b)  $\gamma_{drive}/\omega$  vs.  $\beta_H$  scale length both with FLR and without FLR.

$$dW_{res}/R_{axis} \sim 0.006 - 0.01.$$

In Fig. 14-(a), the peak location of  $\beta_H$  is varied and the drive term is found to increase slowly vs. the location. In experiment, the  $^3\text{He}$  IC resonance is on-axis, so it is reasonable to believe that the peak must be within  $r/a < 0.2$ . In Fig. 14-(b), the scale length of  $\beta_H$  is varied and the drive term dependence is found to be only modestly sensitive.

The total damping rate from NOVA-K, which is independent of the fast ion distribution, is  $\gamma_{damp}/\omega \sim 3.6 \times 10^{-2}$ . The parameter scan shown in Fig. 13 and Fig. 14 shows that at peak  $\beta_{H0} = 0.01$ , the maximum driving term with FLR is  $\gamma_{drive}/\omega \sim 1.1 \times 10^{-2}$ .

For this shot 1160901022, since the driving term at  $\beta_{H0} = 0.01$  is smaller than the damping term, we need to scale up  $\beta_{H0}$  to excite the TAE mode. It gives  $\beta_{crit} = \beta_{H0} \times \gamma_{damp}/\gamma_{drive} = 3.3 \times 10^{-2}$  at  $T_H = 250$  keV.  $\beta_H$  and  $T_H$  need to reach their respective values so that the TAE can be excited.

Experimentally, the  $^3\text{He}$  concentration is deliberately controlled to be at a very low level in order for the 3-ion heating scheme to be effective. It is puffed during the plasma shot and varied carefully shot by shot. As deduced from the mode conversion phenomenon measured by PCI, the  $^3\text{He}$  level for this plasma is  $\sim 1.5 \pm 0.5\%$  [46].

There was no direct measurement of the fast ion temperature in the experiment. In the basic Stix form, the fast ion energy  $T_H \propto [P] T_e^{1.5}/n_{He3}/n_e$ , where  $[P]$  is the volume average RF power density in the region of wave power absorption. Typically  $[P] = 10 \text{ MW/m}^3/\text{MW}_{absorption}$  for on-axis ICRF heating C-Mod (i.e., effective volume for absorption  $\sim 0.1 \text{ m}^{-3}$ ). And using  $^3\text{He}$  concentration of 1.5%, we arrive at  $T_H \sim 400$  keV. Therefore, for this plasma, assuming good

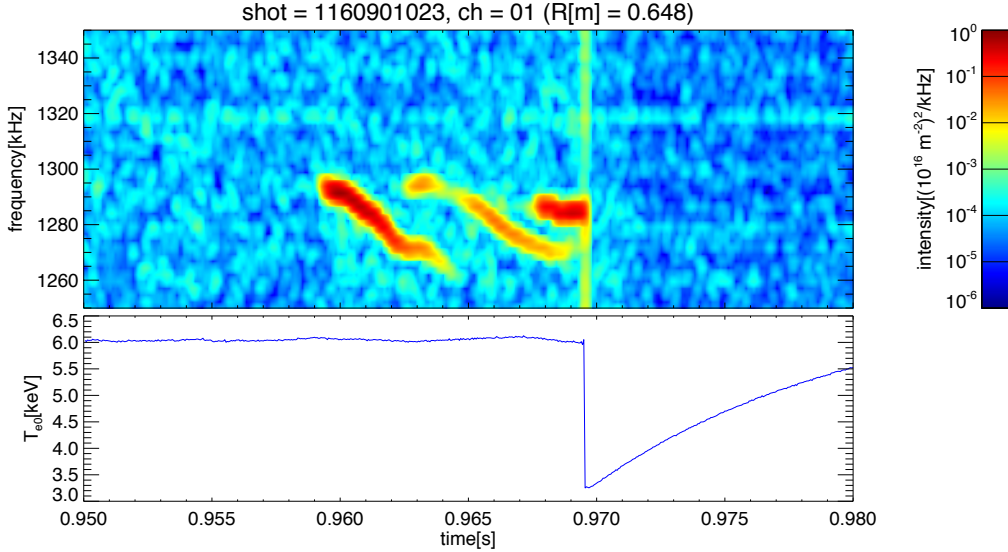


FIG. 15: TAE mode observed in 3-ion ICRF heating experiment (shot 1160901023) on Alcator C-Mod. Top: Spectra from PCI density fluctuations vs. frequency and time. Bottom: time trace of  $T_e$

absorption, tail temperature of 250–300 keV is reasonable to achieve.

However, the maximum  $\beta_H$  is severely constrained. Assuming ALL the fast ions have the energy of the  $T_H = 250$  keV, with the fast ions temperature, density and magnetic field, we have  $\beta_{H0,exp} \leq 0.4\text{--}0.8 \times 10^{-2}$ . It is still a factor of 4–8 lower than the required  $\beta_{crit} \sim 3.3 \times 10^{-2}$  for the TAE to be excited according to NOVA-K calculation.

Fig. 15 shows a different plasma shot where a much higher frequency mode was observed. NOVA-K shows a mode with similar frequency in the EAE gap. Parameter scans show that optimal  $T_H \sim 100$  keV for driving TAE and  $\beta_{crit} = 0.8 \times 10^{-2}$ . However, at this tail temperature,  $\beta_{H0,exp} \leq 0.15\text{--}0.3 \times 10^{-2}$ , which is far too small compared to  $\beta_{crit}$ .

In summary, according to the NOVA-K simulations that have been carried out, these modes are not supposed to appear under the experimental condition.

#### *Discussion and summary of the results*

Lack of direct fast ion measurement and  $q$  profile measurement in the experiment leaves difficulties for a firm interpretation of the simulation result. The damping term calculation from NOVA-K had been compared to the antenna measurement on C-Mod and they broadly agree (within a factor of  $\sim 40\%$ ) [43]. It is also found that the damping term calculation is sensitive to many other parameters like  $q$  profile that was not measured. In Ref. [44], minimum  $\beta_{crit}$  was obtained in NOVA-K by scanning the  $n$  number of TAE mode in ICRF heated plasmas. The minimum  $\beta_{crit} \sim$

$0.3 \times 10^{-2}$  at  $n = -4$  was found to reasonably agree with that estimated from EFIT for the plasma analyzed.

Although  $\beta_{crit}$  is a function of both the driving term and the damping term, the driving term calculation usually is more believable. From experimental evidence, it is more likely that NOVA-K has produced a too high damping rate for these cases. There is continuing work to benchmark damping rate calculations among different codes (e.g. GTC) and to perform inter-machine comparisons [47].

Further analysis of the 3-ion ICRF heating experiment with RF codes will be carried out in the future and it may give some more insight in the RF physics and associated TAE excitation and evolution.

In summary, NOVA-K simulations have been carried out on some Alcator C-Mod plasmas from the 3-ion ICRF heating experiment. The simulation suggests that in the 3-ion ICRF heating experiment,  $^3\text{He}$  ion must have been driven to high energy (hundreds of keVs) in order to trigger the observed TAE activities. This information can be used as the constraint for RF simulation. However, even with the optimized driving term, damping rate from NOVA-K seems to be too high to allow the TAEs to be excited given the experimental constraints. This inconsistency suggests the damping term from NOVA-K may be too high. Further work is needed to resolve the discrepancy.

## E. Improvement of diagnostic and analysis tools

### 1. Development and validation of an Imaging Neutral Particle Analyzer on DIII-D

First images from a novel Imaging Neutral Particle Analyzer (INPA) on DIII-D were reported during the second Quarter of the JRT-18, see Second Quarter Report. The system provides energy and radially resolved measurements of fast ions from the core plasma by measuring charge-exchanged energetic neutrals escaping from the volume illuminating by an active neutral beam source. Neutrals are re-ionized inside the detector by a carbon stripping foil. The tokamak magnetic field then acts as a magnetic spectrometer to disperse the ions on a scintillator plate as a function of the original energy and radial location.

Compared to standard NPA system, the new imaging NPA can cover a broad radial range and energy range with fine resolution. During the last two quarters of FY18, INPA data have been validated for MHD quiescent scenarios against TRANSP simulations [48], confirming the capabilities of the system to provide phase-space resolved measurements of the fast ion distribution and its temporal evolution.

Initial operations identified optimum conditions for INPA measurements. As for other diagnostics based on active charge-exchange techniques, the system has excellent signal-to-noise ratio at low plasma density ( $n \lesssim 3 \times 10^{19} \text{ m}^{-3}$ ), whereas the signal is degraded at higher density because of the increased attenuation of NB neutrals used to probe the core plasma and of increased reionization of the escaping neutrals. For this reason, INPA data did not contribute directly to the main Joint Experiment on DIII-D for the JRT-18 Milestone. However, the INPA is expected to provide

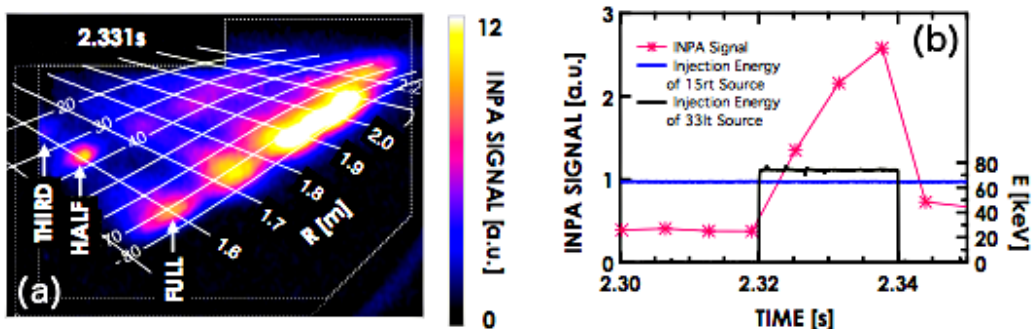


FIG. 16: (a) INPA image across a co-current, nearly-tangential NB blip for DIII-D discharge #173110. (f) Symbols show the time evolution of the integrated signal over the phosphor image. Timing of the background (blue) and active (black) NB sources is shown by solid lines. (Adapted from Ref. [48]).

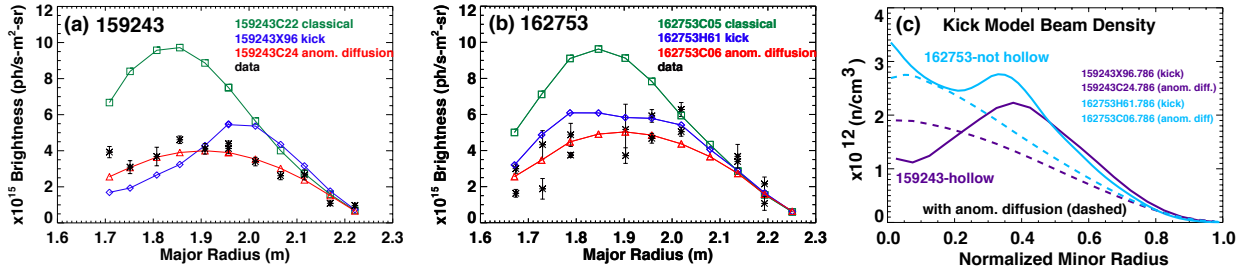


FIG. 17: Revised analysis of FIDA data from DIII-D discharge #159243 based on recent updates in FIDASIM code. This case was compared to shot #162753 with perpendicular beam injection. Here, data for #162753 is analyzed using two different offset values in background subtraction, which results in significant uncertainty in absolute intensity.

valuable additional data e.g. during the current ramp-up/early flat-top phases, which are a good target for fast ion studies on DIII-D.

## 2. FIDASIM analysis for experiment/modeling comparison

Several new capabilities were added to the open-source synthetic diagnostic code FIDASIM [49][9]. With the fast-ion distribution function as input, FIDASIM predicts measured fast-ion D-alpha (FIDA) and neutral-particle analyzer (NPA) signals; it also calculates *weight functions* that relate the fast ion distribution to expected signals. One new capability is the calculation of "passive" FIDA and NPA signals that arise from collisions between fast ions and the cold neutral population at the edge. Another is a framework that can support three-dimensional magnetic fields. Improved parallel processing and numerical methods have significantly reduced computational times. In addition, a rigorous theoretical foundation for weight functions was developed that underlies a new method to infer the distribution from the data called "orbit tomography" [50].

The Fast Ion D-alpha (FIDA) diagnostic is a key tool for EP transport model validation studies, since it provides phase-space resolved measurements of the fast ion profiles. Improvements to streamline the analysis workflow have made it easier to do comparisons between model results and experiment. For example, we can use OMFIT (see Ref. [51] and references therein) to do rapid, multi-timelice profile and equilibrium fitting for input to TRANSP and can now run FIDASIM on the GA computing cluster. As part of testing and workflow development, the kick model validation study was re-visited for the DIII-D reference shot #159243 [7] and a separate case, DIII-D discharge #162753 [52].

FIDASIM was recently updated to use the same beam geometry as TRANSP. Consequently, the 210RT beam source position was moved to larger radius, causing the neutral beam density and calculated FIDA brightness to decrease, especially near the core. The updated results are shown in Fig. 17, where data is compared to interpretive kick model profiles (blue), TRANSP classical results (green) and TRANSP anomalous diffusion (red). Here, anomalous diffusion was applied using a radially invariant, time-varying fast ion diffusivity value to match calibrated neutron data. In order to account for uncertainties in the absolute intensity calibration, the FIDA data at each radius has been multiplied by separate calibration factors that were derived by matching FIDA data to the FIDASIM synthetic signals for a classical shot with no fast ion transport. These calibration factors were the same that were used in Ref. [7].

In Fig. 17, the FIDA brightness profiles, which were generated by integrating spectra over line-of-sight energies  $E = 17.7 - 63.6$  keV, seem to better match the profile from anomalous diffusion. It may be that the large number of overlapping AE resonances causes somewhat uniform transport fast ions across the phase space measured by FIDA. It was pointed out in Ref. [7] that even though the classical signal is larger than the measured signal, the spectra shape predicted by classical calculation agrees well with the experiment, suggesting that AE activity does not appear to cause large distortions in the shape of the velocity distribution function.

The cases in Fig. 17 are interesting to compare because the kick model predicts a hollow beam density profile for #159243, and not hollow profile for #162753 (Fig. 17c). One question is whether there is enough precision in the FIDA data to distinguish between a hollow vs. not hollow profile. In general, the FIDA signal-to-noise ratio decreases towards the core since the neutral beam density decreases towards the core. However, Fig. 17 suggests that the magnitude of the difference between the kick model profiles for the hollow vs. not hollow beam density cases is large enough to distinguish even with large scatter in the FIDA data.

Multiple uncertainties contribute to scatter in FIDA data. One challenge is that each chord is a separate measurement, so channel-to-channel uncertainties can be introduced through issues with absolute intensity calibration, incorrect spatial calibration, as well as unavoidable light scattering issues within the spectrometer. Some of the uncertainties may be eliminated with the new FIDA imaging system that is currently being installed for the upcoming FY-19 run campaign. One recently discovered problem was that the spatial calibration for the FIDA system at the 210RT neutral beam was incorrect. In Fig. 18, the measured FIDA spectrum (purple) is compared to FIDASIM simulated spectrum (green) for the daily reference shot from the 'High-qmin AE Control' experiment day discussed in Sec. G. This shot was MHD quiescent with classical neutrons. In

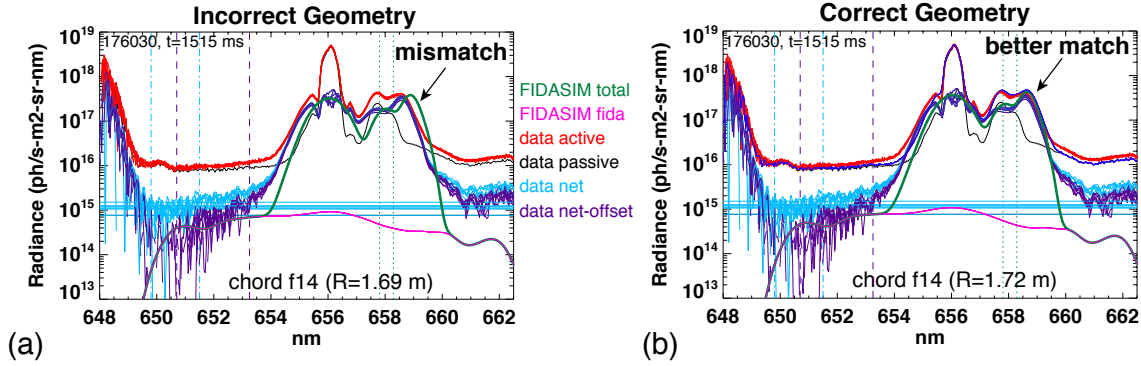


FIG. 18: (a) Comparison of data (purple) to FIDASIM (green) using erroneous chord geometry resulted in an obvious mismatch between predicted and measured beam emission. (b) The corrected geometry results in a better match in beam emission. However, there are still major, unexplained differences in the halo emission and red-shifted FIDA emission. Note that spectral regions for  $\lambda \lesssim 649.5$  nm should be ignored as the apparent increase in emission is an artifact of the bandpass filter.

Fig. 18a, the FIDASIM beam emission is shifted to higher wavelength compared to the measurement. After re-examining the in-vessel geometry measurements, it was discovered that the chords were erroneously shifted 4.1 cm radially inward. Figure 18b uses the correct geometry for the chord location at the midplane, as well as a refined geometry for the chord lens location based on an optics model using the CAD drawings of the fiber and lens system. This results in a better match in beam emission between the data and FIDASIM. The magnitude of the beam emission is in relatively good agreement, however there is significant disagreement in the halo emission and the red-shifted ( $>659.5$  nm) portion of the spectrum. The deficit in FIDASIM halo emission could be due to incorrect plasma profiles, however this deficit is present in a number of different shots. For some of the FIDA chords, excess background light contaminated the red-shifted side of the spectrum. However, the red-shifted FIDASIM prediction is lower than the measured spectra for all chords, which seems to indicate a systematic problem. More work is needed to understand whether these discrepancies are due to issues with hardware or problems with the calculation.

The daily reference shot from the high-qmin AE control experiment day was used as a check for the FIDA absolute intensity calibration, and the FIDA profiles were found to be in relatively good agreement with TRANSP classical run. It should be noted that even if the absolute intensity calibration is well known, a large source of error is introduced through background subtraction. In order to compare the data to the synthetic FIDASIM spectra, the net FIDA measurements are found by subtracting the background spectra when the beam is off (black curve in Fig. 18) from the active spectra when the beam is on (red curve in Fig. 18). Background subtraction is imperfect

because the plasma properties can change with beam modulation, resulting in an elevated net spectrum (blue in Fig. 18). In order to find a true net signal, an offset value (horizontal blue line) is subtracted from the net spectrum, resulting in the final adjusted data (purple) that can be compared to FIDASIM. As shown in Fig. 18, the resulting spectra at each timeslice can be quite noisy in the FIDA spectral region of interest ( $\sim 650 - 653$  nm).

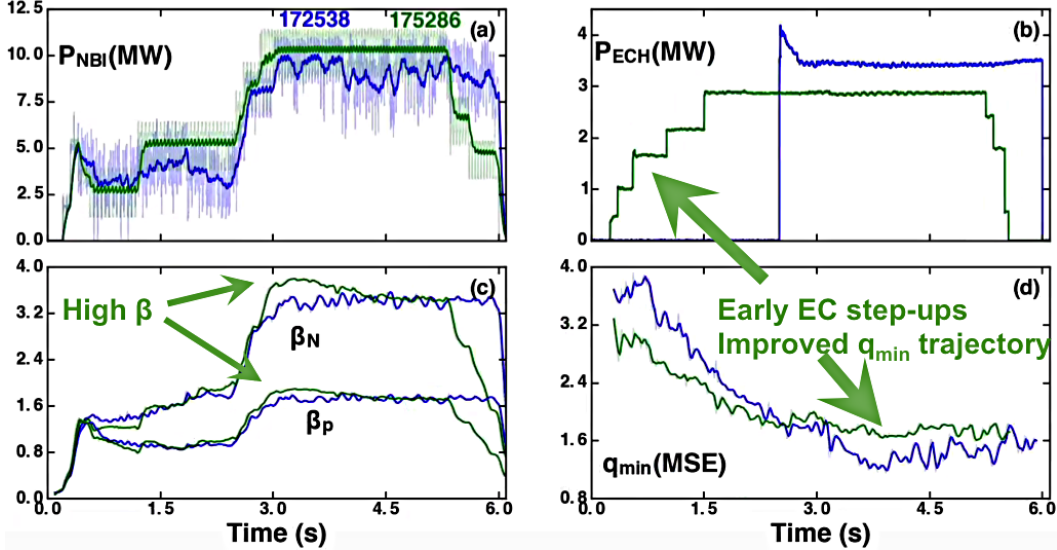


FIG. 19: Illustration of early ECH optimization to achieve reliable access and sustainment of high-min plasmas on DIII-D. Blue traces refer to the reference DIII-D discharge #172538, while green traces refer to the end-product of the optimization process, DIII-D #175286. (a) Waveforms of injected NB power. (b) Waveforms of injected ECH power. Note the early turn-on of ECH for the optimized discharge #175286. (c) Poloidal and normalized beta values,  $\beta_p$  and  $\beta_N$  respectively. (d) Time trace of  $q_{min}$ . Note the long, stationary phase with  $q_{min} \approx 1.7$  achieved for the optimized discharge #175286.

#### F. Validation of scenario predictions in TRANSP

In preparation for the main JRT-18 joint experiment on DIII-D, numerical codes were tested on a set of discharges that had the goal of improving the access to high  $q_{min}$  steady-state scenarios [53][54][66]. In terms of JRT-18 Goals, this exercise provided a first assessment of the overall capability of predicting an entire discharge with minimum prior knowledge of the transport levels and corresponding profile evolution. Whole discharge predictions included the possible destabilization of Alfvénic modes and their effect on EP confinement and losses [67].

In essence, a reference discharge was used as a starting point for predictive TRANSP simulations. Waveforms of the main heating systems, i.e. NBI and electron cyclotron heating (ECH), were varied to improve the (simulated) trajectory of relevant quantities such as  $q$ -profile and plasma beta (ratio of kinetic to magnetic pressure) [54]. During this process, different models for thermal plasma transport were tested and the resulting profiles of electron/ion density and temperature were compared with the actual discharge. From this exercise, the GFL23 thermal transport model was selected as it reproduced satisfactorily well the measured profiles. Note that simulations required a boundary condition for the pedestal height/width, which in this case were computed through the

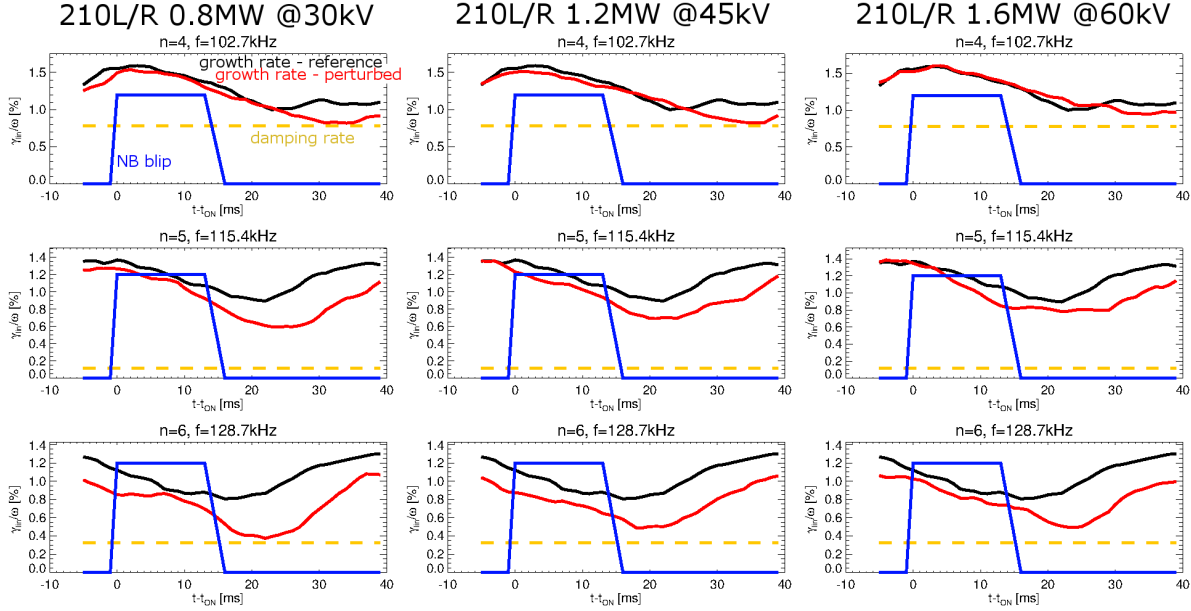


FIG. 20: TRANSP/kick model exploration of using modulation of the counter-current NB sources to mitigate or suppress RSAE/TAE instabilities. The three columns refer to different assumptions on the NB injection voltage and power. For each setting, linear growth rates  $\gamma_{lin}$  are shown for three modes. Modulated NB waveform (blue) and damping rate (yellow) from NOVA-K are shown as reference. Modes would be stabilized for  $\gamma_{lin}$  below the yellow line.

EPED1-NN model based on neural-network representation of predictions from the edge/pedestal model EPED [55]. Figure 19 shows an example of the discharge optimization process on DIII-D. The starting point were previous studies of high  $q$ -min plasmas (e.g. DIII-D discharges #147638 and #172538). In several cases, the trajectory of those discharges was not reliably reproducible, e.g. in terms of  $q$ -profile evolution. TRANSP simulations were then used to study the (predicted) effect of early ECH injection to favor H-mode access and slow down the  $q$ -min drop at early times.

Once an improved set of heating waveforms was identified, stability of EP-driven modes was assessed as further optimization step utilizing the TRANSP/kick model framework. Based on both experimental results an analysis, several AEs are unstable even at the lowest NB power that is required to guarantee a reliable H-mode access,  $P_{NB} \sim 3 - 4$  MW. Net AE growth rates are  $\gamma_{net} \approx 1\%$  or less. Finding ways to reduce the drive for those modes might cause a transition from a "sea of AEs"-type scenario to a plasma with only few unstable modes, which should result in a drastic decrease in fast ion transport and consequent improvement in performance [56][57]. To test this possibility, variations of the NB mix were explored through TRANSP assuming the same equilibrium and background profiles as in the reference (*optimized*) case, see Fig. 20. As a

practical constraint, most of the NB sources are already used in the reference discharge except for the counter-current beams. The latter need to be modulated as "diagnostic beams" for some of the fast ion systems in the real experiment. Therefore, the effects of a similar modulation with varying NB injection voltage and power (at constant current) were investigated to check whether parameters could be optimized to stabilize or mitigate TAEs and RSAEs. As shown in Fig. 20, although the analysis predicts a stabilizing effect on the AE modes, stabilization is not enough to suppress the modes entirely. (Since these NB sources are aimed counter-current, a further increase in power would likely result in an overall decrease in NB current drive efficiency and slow down rotation - both undesired effects in this case). Although no clear AE suppression strategy could be identified, this predictive study was nevertheless useful in terms of run time optimization, for example to give higher priority to other AE mitigation techniques that aim at modifications of the AE continuum structure or at increasing the damping rate by varying thermal plasma density [58].

The set of heating waveforms obtained from simulations was finally used as starting point for the real experiment [54], cf. results from DIII-D discharge #175286 in Fig. 19 [59]. Further refinements to the heating power waveforms led to the initial conditions for the main JRT-18 joint experiment [58], see Sec. G below.

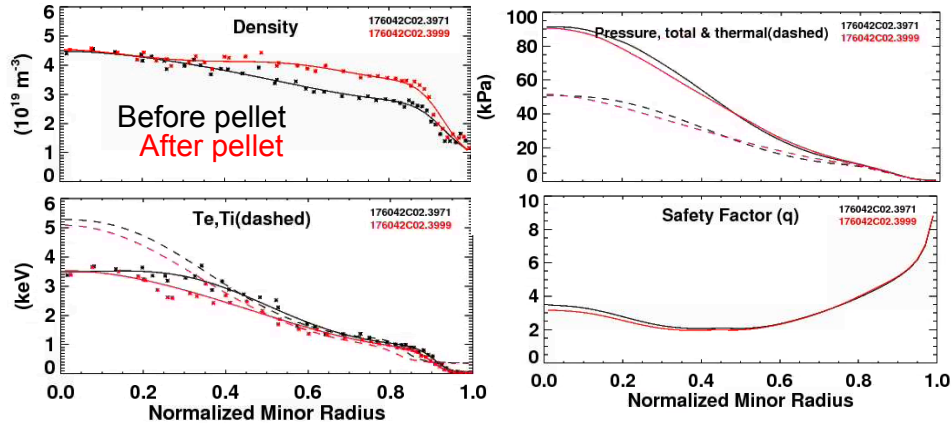


FIG. 21: Profiles of density, temperature, pressure and safety factor around  $t = 4000$  ms for DIII-D #176042.

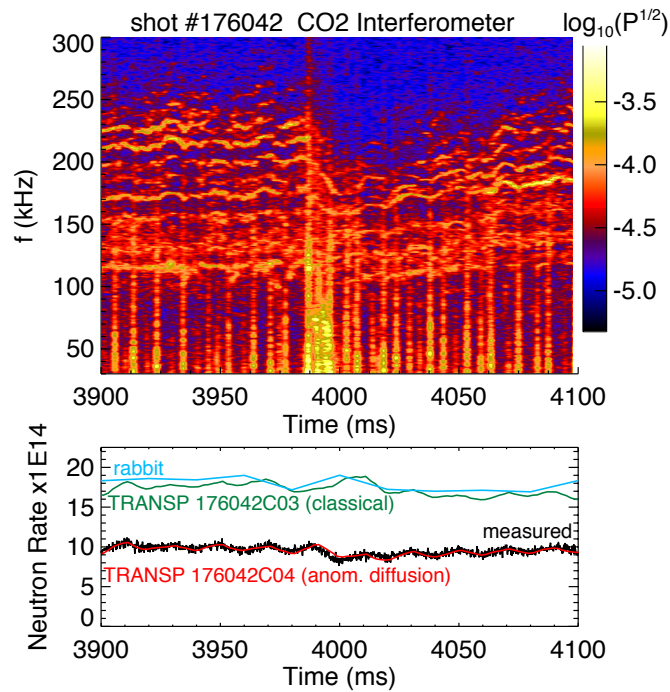


FIG. 22: Top: spectrum of density fluctuations measured through interferometry for DIII-D discharge #176042. The change in the observed fluctuations around  $t = 4000$  ms is caused by injection of a large pellet that modifies plasma density and temperature. Bottom: neutron rate from TRANSP and from the RABBIT code [60].

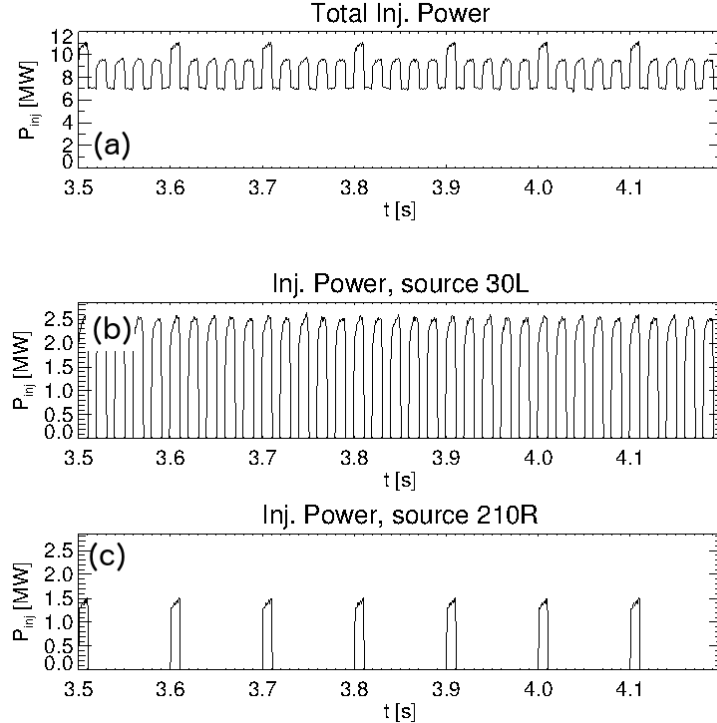


FIG. 23: Waveforms for (a) total injected NB power for DIII-D #176042 and (b,c) for two NB sources with modulated power.

## G. Steady-state high $q$ -min scenario for AE studies on DIII-D

### 1. DIII-D discharge #176042

DIII-D discharge #176042 from the joint JRT-18 experiment is used as reference for most of the analysis discussed in the following Sections. The target is a steady-state high  $q$ -min scenario. Previous work has indicated a substantial degradation in performance caused by Alfvénic activity [61][62][56], which motivated a dedicated experiment in FY-18 to explore strategies for AE suppression/mitigation [58].

Plasma profiles around the time of interest,  $3800 \leq t \leq 4200$  ms, are shown in Fig. 21. During the flat-top, the safety factor has a reversed shear with  $q_{min} \approx 2$ . The injected NB power is  $P_{NB} = 7 - 10$  MW, which provides the drive for a large number of Alfvénic instabilities (Fig. 22). Fast ion transport is enhanced with respect to the neoclassical level, as inferred from the drop in neutron rate compared to classical TRANSP simulations. Waveforms of the injected NB power are shown in Fig. 23. Two NB sources are modulated for diagnostic purposes, with a 10 ms ON time and duty cycle of 50% and 10%. Details of the NB injection geometry are given in Fig. 24.

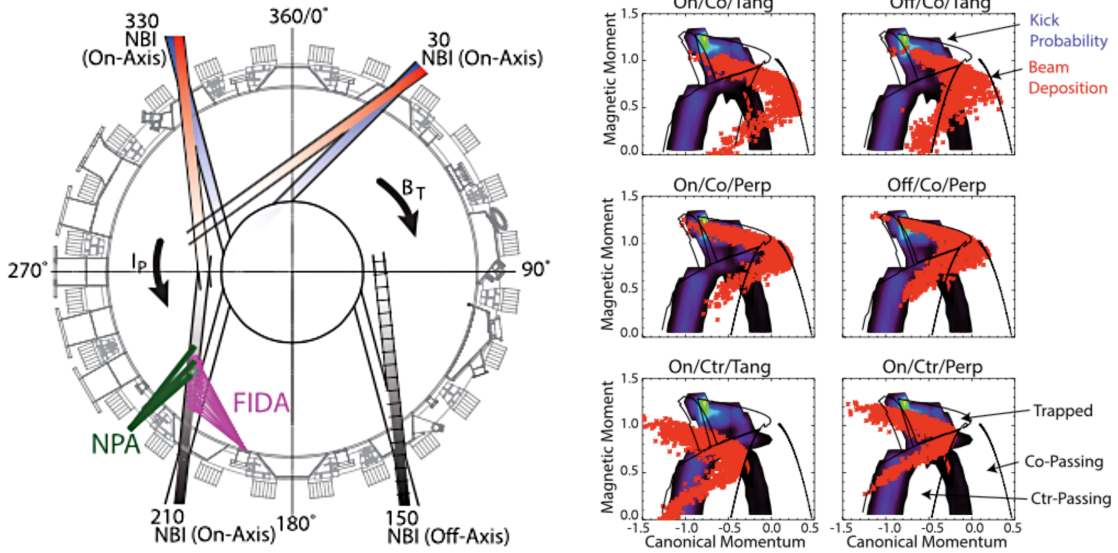


FIG. 24: Left: elevation of DIII-D showing the injection geometry for the available NB sources. Right figures show typical deposition locations in phase space (red symbols). Contours represent the root-mean-square energy kicks from NTM instabilities. (Adapted from Ref. [63]).

## 2. Predictive EP transport modeling

The full predictive analysis for AE instabilities includes four main steps:

- MHD analysis to identify candidate AE eigenmodes
- Stability analysis to down-select a subset of unstable Alfvénic modes
- Analysis to infer the saturated mode amplitude
- TRANSP runs including reduced EP transport models to assess (i) the impact of AEs on EP transport and confinement, and (ii) validate the models results against available experimental data

The following subsections discuss results from each of those steps based on data from DIII-D discharge #176042.

### *Linear stability analysis and selection of the unstable AE spectrum*

RBQ-1D and kick model analyses are based on the same set of NOVA-K runs. The latter provide radial mode structure and damping rates for an initial, broad set of candidate eigenmodes. For DIII-D discharge #176042, about 60 candidate eigenmodes with  $n = 1 - 8$  are identified over a broad frequency range,  $f = 50 - 300$  kHz.

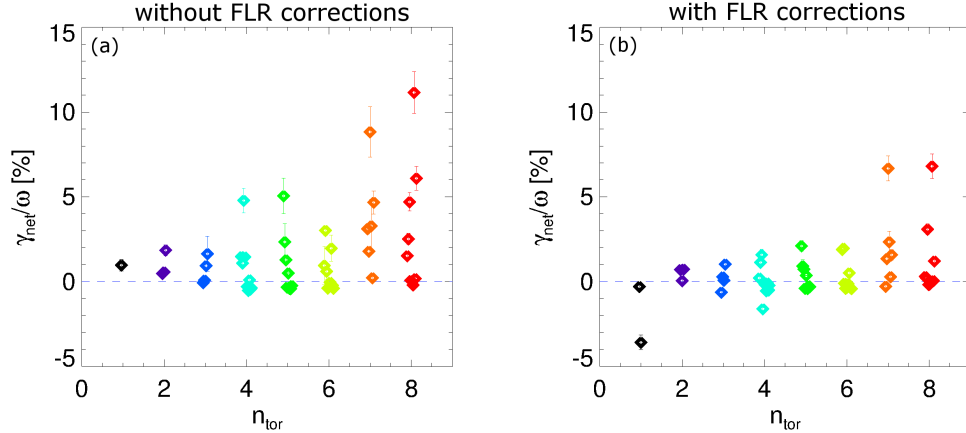


FIG. 25: Net linear AE growth rate from kick model stability analysis for DIII-D #176042. Colors identify different toroidal mode numbers. (a) Computed rates neglecting finite Larmor radius (FLR) effects. (b) Rates computed with a simplified model to include FLR effects in the ORBIT gyro-center code. The computed reduction in growth rate is more significant as the toroidal mode number increase and modes structures become more localized.

Linear stability analysis is then performed to down-select a subset of *dominant* modes, i.e. the modes with the largest net growth rate,  $\gamma_{net}$ , obtained as the difference between the growth damping rates ( $\gamma_{gr}$  and  $\gamma_{damp}$ , respectively). Figure 25 shows the stability results from the kick model over the selected toroidal mode number range. Indeed, a large number of modes are predicted to be *linearly* unstable.

It should be noted that the standard kick model analysis does not include finite Larmor radius (FLR) effects on the wave-particle interaction. Although results without FLR corrections are shown in the following, it is instructive to assess how stability would be modified with those corrections. To this end, the ORBIT code has been modified to enable radial averaging of the perturbation experienced by particles over their gyro-motion to mimic FLR effects. The outcome in terms of linear stability is shown in Figs. 25b and further discussed in Fig. 26. As expected, a reduction by a factor 2 – 4 is observed in  $\gamma_{net}$  (Fig. 26d). As a further verification, linear growth rates from the kick model are compared with rates computed through NOVA-K that include FLR effects, see Fig. 26. Increase in growth rate if FLR effects are neglected is confirmed and a better agreement between kick and NOVA-K is observed when both models apply FLR corrections. (A perfect agreement should not be expected since the two models use different fast ion distribution functions to compute the mode drive). In spite of the measurable effects on linear stability, additional tests have shown little effects on the inferred saturation amplitude. Those corrections are therefore not included in the following, enabling shorter computing time.

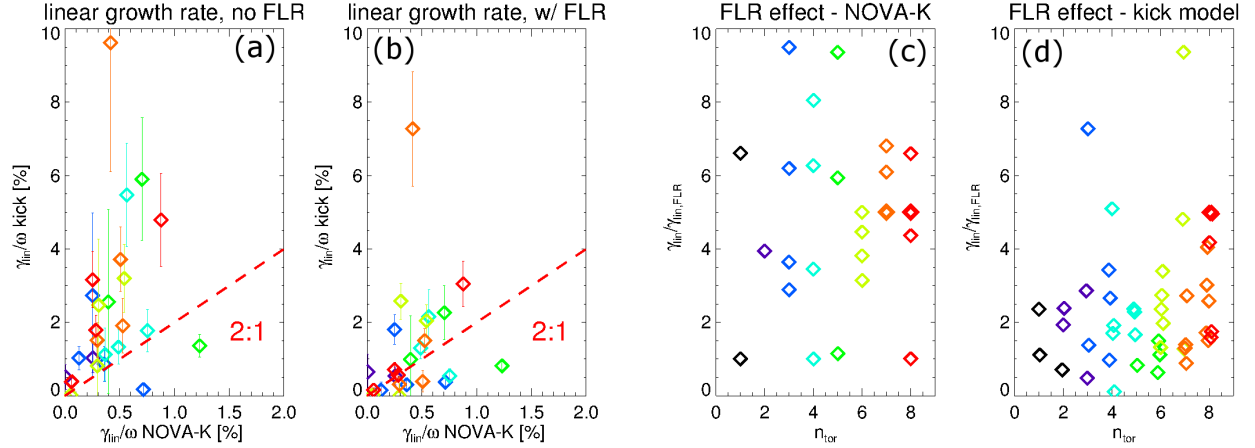


FIG. 26: Comparison between linear growth rates from the kick model and from the NOVA-K code when FLR effects are (a) neglected or (b) included in the kick model. Colors identify different toroidal mode numbers. To guide the eye, the red dashed line indicates where growth rate from the kick model is twice the growth rate from NOVA-K. (c,d) Ratio of growth rate with/without FLR corrections from NOVA-K and kick model, respectively, as a function of toroidal mode number.

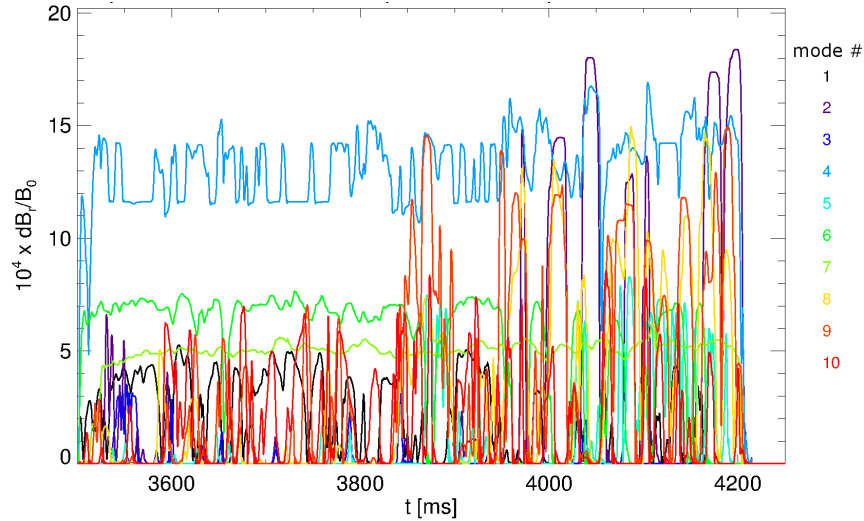


FIG. 27: Saturated amplitude as a function of time computed through the kick model in TRANSP for 16 Alfvénic modes. Some of the curves represent the joint evolution of multiple modes.

#### *Mode amplitude near saturation*

Based on the selected set of most (linearly) unstable modes, the expected saturation amplitude is computed. For the kick model, this requires a series of TRANSP runs in which the amplitude of each mode is gradually increased until the inferred mode drive (from NUBEAM) matches the damping rate from NOVA-K at each time of the simulation. Results for a set of 16 modes are shown in Fig. 27

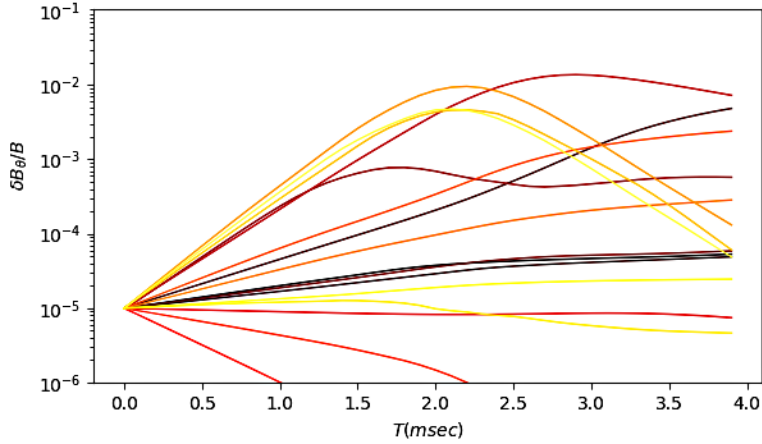


FIG. 28: RBQ-1D self-consistent evolution of 11 Alfvénic modes, including RSAE and TAE modes. The time around  $t = 2$  ms, at which the larger-amplitude modes are near saturation, corresponds to the time used to evaluate the diffusion coefficients of beam ions. Stable modes whose amplitude decays in time can be identified and removed from further analysis.

$n$	3	4	4	4	4	4	5	5	5	6	6	6	7	7	8	8
$f[\text{kHz}]$	102.5	148.7	179.3	242.5	255.4	104.8	155.9	255.4	114.4	174.8	276.8	283.2	185.1	282.8	139.4	182.7
$10^4 \times \delta B_r^{\text{peak}}/B_0$	24.7	3.7	0.7	0.0	0.0	2.6	37.8	0.0	24.8	5.3	1.7	17.4	1.6	0.0	4.8	2.4

TABLE I: Predicted saturation amplitudes from RBQ-1D. Stable modes are indicated by a zero amplitude. Note that amplitudes are converted from the surface perturbation,  $\delta B_s/B_0$ , shown in Fig. 28 to the radial perturbation  $\delta B_r/B_0$ .

in terms of peak value of the radial magnetic field perturbation,  $\delta B_r/B_0$  as a function of time. Inferred saturation values show a large variability among modes, with  $10^{-4} \lesssim \delta B_r/B_0 \lesssim 1.5 \times 10^{-3}$ . These values are comparable from what previously measured on DIII-D [7] using the radial ECE system. However, initial analysis of the available fluctuation data suggests that experimental values for this case might be consistently larger than the predicted amplitudes, see Sec. G 3.

The method used to infer the saturated mode amplitudes in RBQ-1D is substantially different from what is done for the kick model. As a result of the code improvements made during the first three Quarters of FY-18, the RBQ-1D model can now infer saturation amplitudes by evolving a set of AEs and the resulting fast ion distribution simultaneously, see Fig. 28. This method allows to quickly identify dominant modes as well as stable modes whose amplitude decays in time. Since RBQ-1D does not include sources and sinks, gradients in the fast ion distribution will eventually flatten at the resonance location and the mode drive will stop. Therefore, the final saturation amplitude is inferred for each of the unstable mode from the time at which the mode evolution

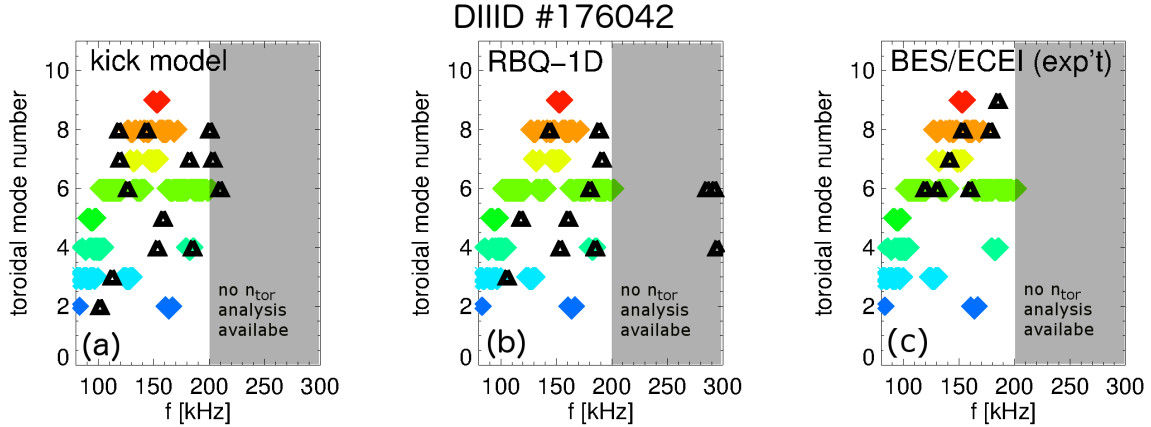


FIG. 29: Comparison of measured toroidal mode number spectrum as a function of frequency (colored symbols are used to differentiate different mode numbers) with predicted spectrum from (a) kick model and (b) RBQ-1D linear analyses, shown as black symbols. (c) Black symbols show frequency and mode number of modes for which a good match between NOVA-K eigenmodes and experimental data from BES is obtained. Only (linearly) unstable modes are shown for the kick and RBQ-1D predictions.

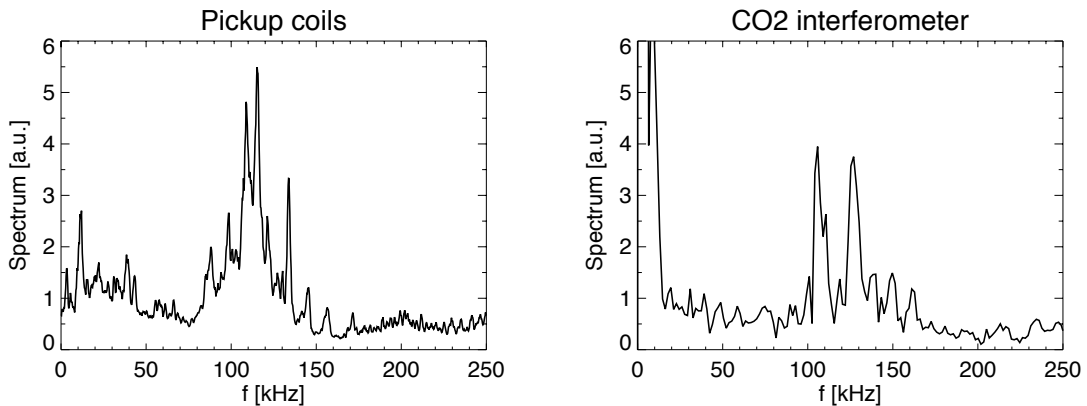


FIG. 30: (a) Magnetic fluctuation spectrum from Mirnov coils. (b) Density fluctuations from a vertical interferometer chord intersecting the mid-plane around mid-radius.

shows an inflection point and starts to decrease after the initial growth. For the example in Fig. 28 this time is between 2 ms and 3 ms for most modes.

As reported in Tab. I, the inferred saturated amplitudes from RBQ-1D are  $10^{-4} \lesssim \delta B_r / B_0 \lesssim 2.5 \times 10^{-3}$ , which is in fair agreement with the kick model results.

#### *Predicted unstable AE spectrum*

Although kick and RBQ-1D models give similar estimates for the saturated AE amplitudes, the sets of modes identified by the two models differ, probably as a result of the different methodology

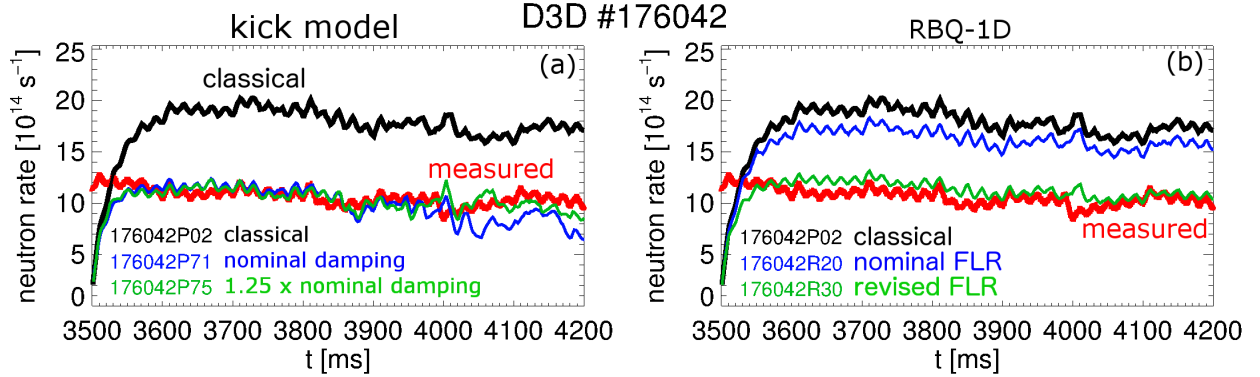


FIG. 31: Neutron rate predictions from (a) kick model and (b) RBQ-1D models. Measured neutron rate is shown in red. Classical predictions are shown in black.

used to compute the initial linear stability and down-select the most unstable modes. A comparison between the mode spectrum from the two models is shown in Fig. 29. When compared with experimental measurements of the toroidal mode numbers, the two models recover the broad spectrum of instabilities observed in the experiment. Only a partial agreement with the experiment is achieved in terms of *both* toroidal mode number and frequency. Several modes predicted by either model lie at frequencies where no corresponding mode with the same  $n$  is measured. Unfortunately, no mode number identification is available from the experiment for frequencies  $\gtrsim 200$  kHz, which would have been useful for example to confirm the presence of  $n = 4, 6$  modes around  $f \sim 290$  kHz predicted by RBQ-1D but not found from the kick model.

In addition to the predictions from the models, Fig. 29c also shows a set of modes for which a positive identification is obtained between experimental mode structure, frequency and mode number data and specific eigenmodes calculated by NOVA. Notably, no good match was obtained for mode numbers  $n \leq 5$ . The reason can be understood by comparing the fluctuation spectrum from BES and interferometer data with the spectrum from magnetic pickup coils, see Fig. 30. Whereas no significant activity is detected from systems measuring in the plasma core, pickup coils show a rich spectrum at frequencies  $\lesssim 100$  kHz. Those peaks are likely caused by (possibly non-Alfvénic) edge fluctuations, which do not appear on BES data. The fact that unstable AEs are instead predicted by both kick and RBQ-1D model is further discussed in Sec. H.

#### *Predicted neutron rate deficit*

The first, obvious application of the inferred AE mode spectrum and saturation amplitudes is their inclusion in TRANSP/NUBEAM to compute the predicted neutron rate degradation caused

by enhanced NB ion transport by AEs. The results from both kick and RBQ-1D models are summarized in Fig. 31. Kick model predictions are clearly close to the measured neutron rate, which is on average reduced by  $\approx 40\%$  with respect to classical simulations. The simulation appears well-behaved up to  $t \approx 3900 - 4000$  ms, after which oscillations in the kick predicted rate are seen. Oscillations are caused by large spikes in the predicted saturation amplitudes, cf. Fig. 27. Nevertheless, the predicted neutron rate is in much better agreement with measurements than the classical prediction. Improvements in the kick predictions can be achieved by postulating a slight increase of 25% in the modes' damping rate, which is well within uncertainties from NOVA-K calculations.

Results from RBQ-1D are shown in Fig. 31b. When the standard NOVA-K algorithm to include FLR effects is used, the model under-predicts the measured neutron rate. However, when a revised procedure is adopted (neglecting corrections based on the mode radial wave-number), the agreement improves considerably. In practice, the main effect of modifying the FLR corrections is to reduce the damping rates and therefore increase the predicted saturation amplitudes to the levels shown in Fig. 28 and Tab. I.

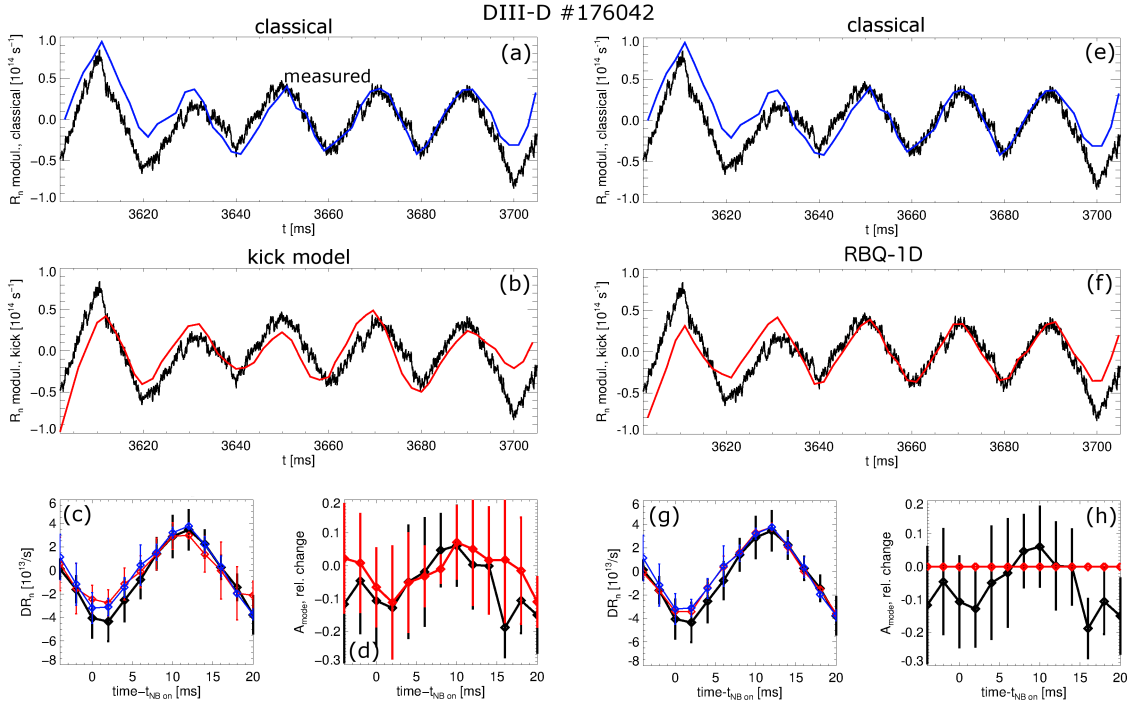


FIG. 32: Analysis of neutron rate response to NB modulation from (a-d) kick and (e-h) RBQ-1D models. Top panels show the neutron rate modulation from classical (blue) and kick/RBQ-1D simulations (red). Measured neutron rate is shown in black. Bottom panels show the conditionally-averaged response to modulation of (c,g) neutron rate and (d,h) mode amplitude from experiment and kick modeling. Mode amplitude is kept constant in time for RBQ-1D. Error bars indicate the standard deviation of the conditional average samples.

### *Predicted response to NB modulation*

In addition to the agreement with the measured neutron rate, the dynamical response of fast ions and instabilities to variations of the injected NB power provides valuable information on the accuracy of EP transport models [64]. For the discharge under consideration, the main contribution (typically  $\sim 90\%$ ) to the measured neutron rate comes from beam-target reactions between fast ions near the NB injection energy and the thermal deuterium ions. Hence, the neutron rate response to NB modulation - and its deviations from classical behavior - is representative of the transport of NB ions deposited in regions of EP phase space, depending on the NB injection geometry. Two NB sources are modulated during the time of interest for DIII-D discharge #176042, cf. Fig. 23. In particular, the modulated  $30L$  source deposits trapped, stagnation and co-passing particles (Fig. 24).

Results from the analysis of the neutron rate response to NB modulation are shown in Fig. 32. The selected time window corresponds to early times in the simulation time range. Both kick

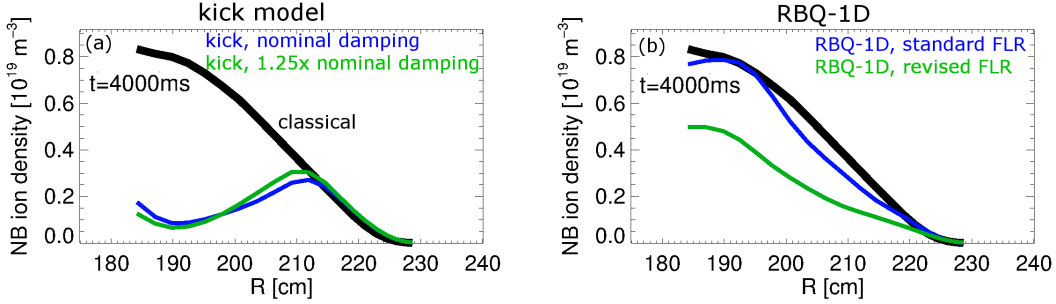


FIG. 33: Fast ion density profiles at  $t = 4000$  ms from TRANSP simulations with enhanced fast ion transport via (a) kick model and (b) RBQ-1D.

and RBQ-1D models show a reasonable match with the conditionally-averaged measurements (Figs. 32c,g) and with the classical simulation results. (Discrepancies are most likely due to jitter caused by the finite time step used in the simulation,  $t_{step} = 2$  ms combined with the coarse 1 ms time grid over which the TRANSP input waveform is defined).

For the kick model, which aims at predicting *time-dependent* mode amplitudes, an additional useful comparison is available from the measured vs. predicted variations in mode amplitude as the NB power is varied (Fig. 32d). The comparison with available experimental data is positive. Both simulation and experiment suggest a  $\approx 10\%$  modulation in the mode amplitude as the NB power is increased, although variability between different modulation cycles is significant. At later times,  $t > 4000$  ms, the agreement is less favorable. Experimental data still indicates a modulation of the mode amplitude, which is not observed in kick simulations. As previously noted, however, the computed mode amplitudes are questionable in the latter part of the simulation and no clear conclusions can be drawn.

#### *Predicted fast ion profiles and fast ion distribution*

As a final comparison between the results from the two models, the computed NB ion density profiles are shown in Fig. 33 for the same simulations as in Fig. 31. Unlike for the neutron rate and response to NB modulation, the results from the two models are strikingly different. The kick model predicts an hollow density profile with a large central depletion of fast ions with respect to classical simulations, see Fig. 33a. Similar results are obtained by increasing the nominal damping rates from NOVA-K by 25%, which helps reducing spikes in the mode amplitudes for  $t > 4000$  ms. In contrast to the kick model results, RBQ-1D results in peaked profiles with a much less significant depletion (Fig. 33b). Peaked profiles persist when mode amplitudes are calculated using a revised calculation of the FLR effects on the damping rate.

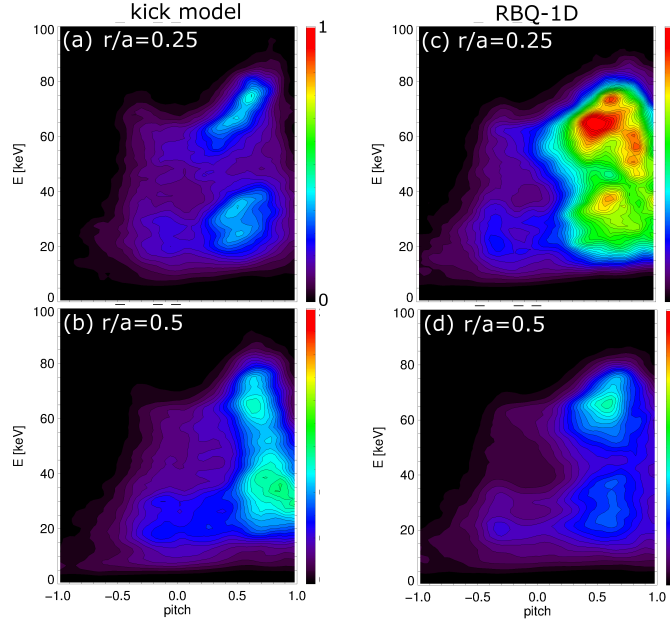


FIG. 34: Fast ion distribution from kick (left column) and RBQ-1D (right column) at two different radii. The same color scale is used for all contour plots.

Examples of fast ion distribution functions for the nominal kick and RBQ-1D simulations are shown in Fig. 34. As expected, the kick model distribution is strongly depleted near the core. Levels are comparable outside mid-radius, where the kick model predicts a higher density of trapped and co-passing particles than RBQ-1D.

#### *Reconstructed FIDA response and comparison with experiment*

Based on the simulated fast ion distributions, the FIDASIM code is used to compute the expected FIDA brightness profile for a direct comparison with the experiment. The results are shown in Fig. 35. It is clear that neither model can reproduce the measured profile across the entire major radius. RBQ-1D is in reasonable agreement with the experimental profile near and inside the magnetic axis ( $R \approx 1.8$  m), but it over-predicts transport in the outer plasma regions. The kick model shows the opposite trend, with a reasonable match to the experiment at the edge but a large over-prediction of the core EP transport.

In addition, two important details emerge when FIDA spectra are divided in two energy ranges, see Fig. 36. First, none of the models (including the ad-hoc anomalous diffusivity) agrees with the experimental data at all radii and for both energy ranges. Second, low energy spectra appear to be at near-classical levels, which seems to be incompatible with the large depletion of NB ions at in the higher energy range. These observation suggest two important conclusions:

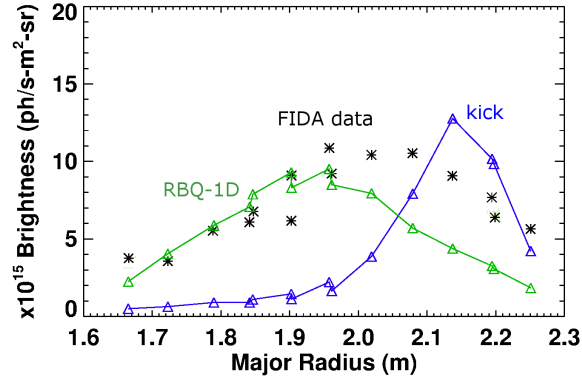


FIG. 35: Comparison of experimental FIDA brightness profile vs the profile reconstructed through FIDASIM for kick and RBQ-1D model results.

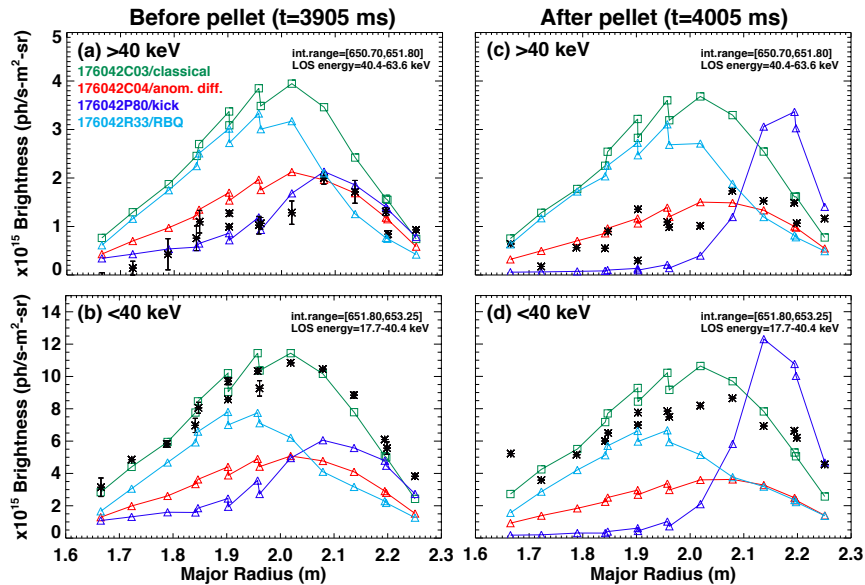


FIG. 36: Comparison of experimental FIDA brightness profile vs the profile reconstructed through FIDASIM for kick and RBQ-1D model results. In the anomalous diffusion model, an anomalous fast ion diffusivity of  $D_b \sim 3.5 \text{ m}^2/\text{s}$  was used to match the measured neutron rate.

- The reasons for discrepancy between kick and RBQ-1D models need to be understood for a meaningful assessment of the codes' capabilities. Progress has been made in this direction, as discussed in Secs. G 3 and H.
- Additional work is required to improve confidence in - and reliability of - the analysis of experimental data from phase-space resolved diagnostics such as FIDA, as already observed in Sec. E 2.

### 3. Interpretive EP transport modeling

The comparison between NOVA-K results for candidate eigenmodes at  $t = 3950$  ms and experimental data from BES provides a set of candidate modes to be used for interpretive kick model analysis. Toroidal mode number spectrum, frequency and inferred peak amplitude of the resulting set are summarized in Fig. 29c and Tab. II. The set includes 4 TAE modes and 3 RSAE modes, with RSAEs more core localized.

Interpretive TRANSP results that use the inferred modes and 'experimental' amplitudes in the kick model are shown in Fig. 37. As a first step, the ORBIT analysis that provides the input transport matrices for TRANSP/NUBEAM does not include FLR corrections. The large amplitudes inferred from the experiment,  $\delta B_r/B_0 = 1-5 \times 10^{-3}$ , result in an overestimated neutron rate deficit. NB ion density profiles are flattened over the entire radius.

The simulation was repeated assuming reduced mode amplitudes to achieve a better agreement with the measured neutron rate. In this case, TAE amplitudes are  $\approx 15\%$  of their nominal value. RSAE amplitudes are further reduced to  $\sim 10\%$  of the nominal value to maintain a near-zero net power flowing from the fast ions to the modes. Larger RSAE amplitudes cause the power to become negative, indicating that modes would be *stabilized* by the fast particles. A reduction in transport is expected when FLR corrections are introduced in the kick model. This is demonstrated in Fig. 37, which also shows the high sensitivity of the NB ion density profiles to different assumptions on the underlying transport (e.g. by neglecting or including FLR effects, in this case). The reduction in transport is caused by reduced energy and  $P_\zeta$  kicks experienced by fast ions once FLR corrections are introduced in ORBIT. Figure 38 shows representative sections of phase space at constant energy and the corresponding average energy kicks caused by a TAE mode. Kicks are reduced as the variable  $\mu B_0/E$  increases at constant energy, moving from strongly co-passing particles ( $\mu B_0/E \rightarrow 0$ ) to trapped/stagnation orbits for  $\mu B_0/E \gtrsim 1$ .

Comparison between the simulated fast ion distribution and the resulting FIDA signal from FIDASIM is planned, similarly to what shown in Fig. 35 for the predictive simulations.

$n$	6	6	7	8	6	8	9
$f[kHz]$	152.3	166.7	180.5	195.6	204.2	227.2	236.0
$10^4 \times \delta B_r^{peak}/B_0$	5.86	10.4	12.42	18.95	6.44	11.45	16.5

TABLE II: Summary of modes identified by comparing NOVA-K eigenmode structures to BES measurements. The reported  $\delta B_r/B_0$  are the peak values of the radial perturbation.

## H. Interpretation of the JRT-18 results: resolving the RBQ-1D vs. kick discrepancy

One of the main outcomes from the predictive simulations with the kick and RBQ-1D models (Sec. G 2) is the large discrepancy between predicted NB ion density profiles, cf. Fig. 33. This Section explores the possible reasons for the discrepancy. Specific physics mechanisms that are included in one model, but are missing in the other one, are identified, thus providing hints for possible extensions of the models. In particular, three key physics elements have been identified:

- Initial prediction of the spectrum of most unstable modes.
- Diffusive approximation in RBQ-1D, based on quasi-linear theory.
- Inclusion of finite electrostatic potential effects.

Those three aspects are reviewed in the following paragraphs, showing how the two models do provide similar predictions once simulations retain the same physics.

### *Initial prediction of the most unstable modes*

Figure 39 compares the results from the kick model predictive simulations of DIII-D #176042 with equivalent results obtained using the set of AE modes that is predicted by RBQ-1D (cf. Fig. 30). When the analysis is repeated using the set of modes from RBQ-1D, the predicted drop in neutron rate is slightly reduced. Notably, the resulting NB ion density profile is much flatter (with hints of central peaking) than for the initial kick model simulations. The qualitative

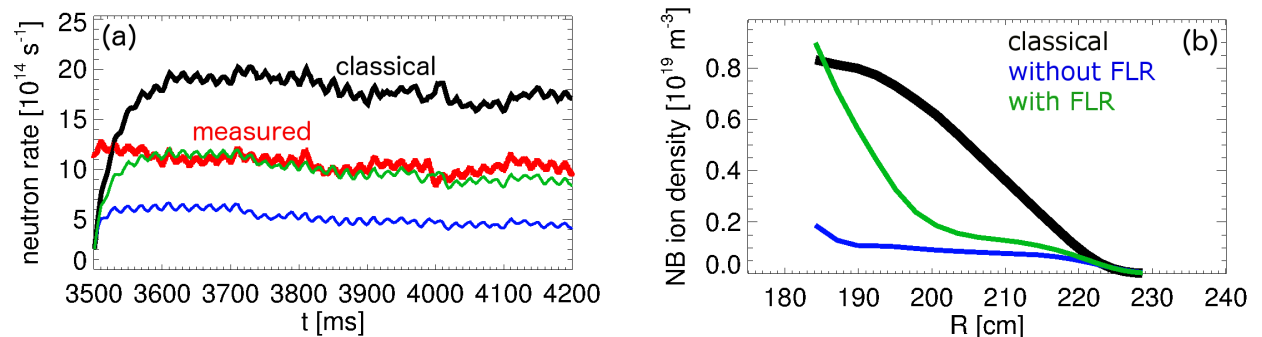


FIG. 37: (a) Neutron rate from kick simulations using the nominal mode amplitudes inferred from the experiment. Blue curves refer to simulations for which FLR corrections are not included to compute the transport probability matrices. Green curves are obtained by including FLR corrections. Measured and classical neutron rates are shown for comparison. (b) Corresponding NB ion density profiles at  $t = 4000$  ms.

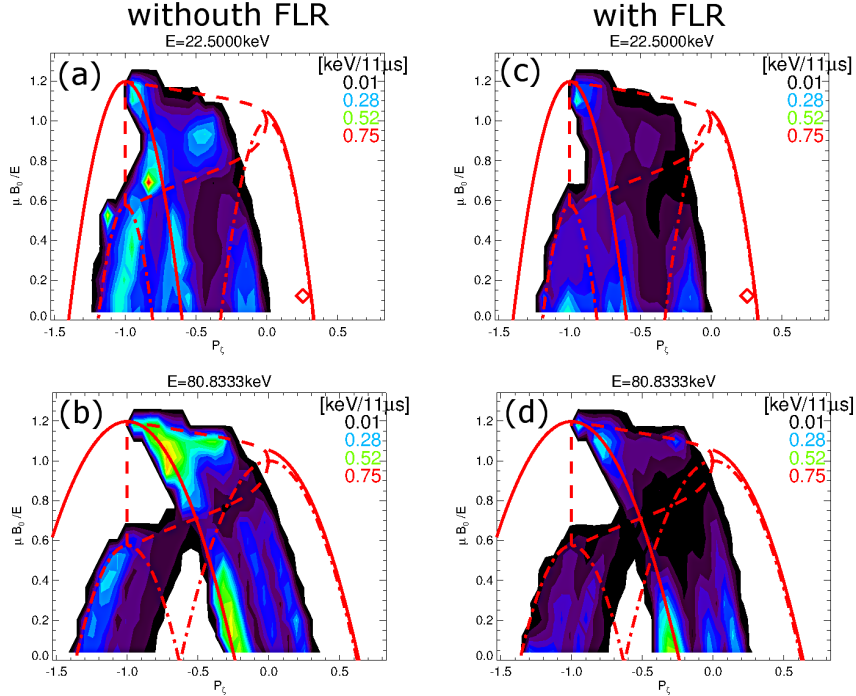


FIG. 38: Average energy kicks in phase space at two representative fast ion energies computed for a TAE transport probability matrix from ORBIT. Left column: FLR corrections are neglected in ORBIT. Right column: FLR corrections are included.

agreement between the two models further improves if only seven (dominant) poloidal harmonics are retained in the analysis, as is done in the RBQ-1D calculations. In this case, the kick model also computes peaked NB ion densities, although in this case the neutron rate deficit is only  $\approx 50\%$  of the measured one.

These simulations retain the two-dimensional transport capability in energy and canonical momentum that characterizes the kick model. The estimated power flowing from fast ions to the modes can thus be compared for the three cases, showing only a modest reduction when modes from RBQ-1D are used. The main conclusion from this comparison is that sub-dominant poloidal harmonics do not play a major role in the overall mode stability (power transfer is comparable), but they can affect fast ion transport quite considerably. In fact, previous studies reached a similar conclusion [65]. This indicates the necessity, especially for low- $n$  modes, of retaining a large number of poloidal harmonics to properly account for fast ion transport when multiple instabilities act simultaneously.

#### *Diffusive approximation in RBQ-1D*

Figure 40 compares the NB ion density profile from RBQ-1D with the profiles computed by the

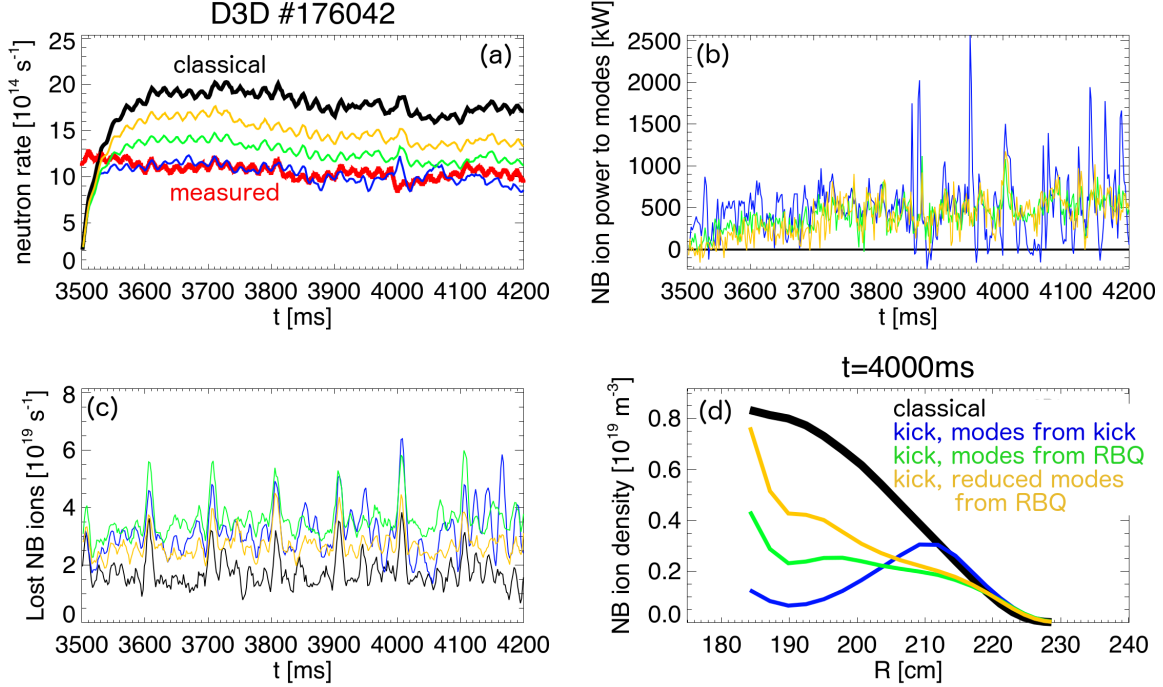


FIG. 39: TRANSP/kick model results for (a) neutron rate, (b) power from fast ions to the modes, (c) fast ion losses and (d) NB ion density profile at  $t = 4000$  ms using different sets of AE modes. Blue curves show results using the most unstable AEs from linear stability analysis through the kick model. Green curves are obtained using the set of modes predicted to be unstable by RBQ-1D analysis. Yellow curves are obtained using the modes from RBQ-1D, limiting the calculations to only seven poloidal harmonics for each mode as done in RBQ-1D.

kick model using the same set of modes and a reduced number of poloidal harmonics. Although the agreement is not perfect, it should be noted that the two models have different assumptions on the transport process for fast ions. Since its transport probability matrices are computed numerically through ORBIT, the kick model does not make assumptions on the nature of transport, which can be any combination of sub/super-diffusive transport or even convective transport (depending on the phase space locations). Therefore, some differences can be expected. Differences are expected to be further enhanced by the finite grid size over which the  $\Delta P_\zeta$  kicks in canonical momentum are defined. Resonant islands have a limited width in  $P_\zeta$ , but the diffusive approximation - implying a gaussian  $p(\Delta P_\zeta)$  kick probability - forces non-zero (although small) transport beyond the island boundaries. A finite  $\Delta P_\zeta$  grid will naturally clip some of the (unphysical) transport contributions at large  $\Delta P_\zeta$  values, with the exact amount of excluded 'transport' now becoming a function of the selected grid boundaries.

As a next step, energy transport is turned off in the kick model and canonical momentum

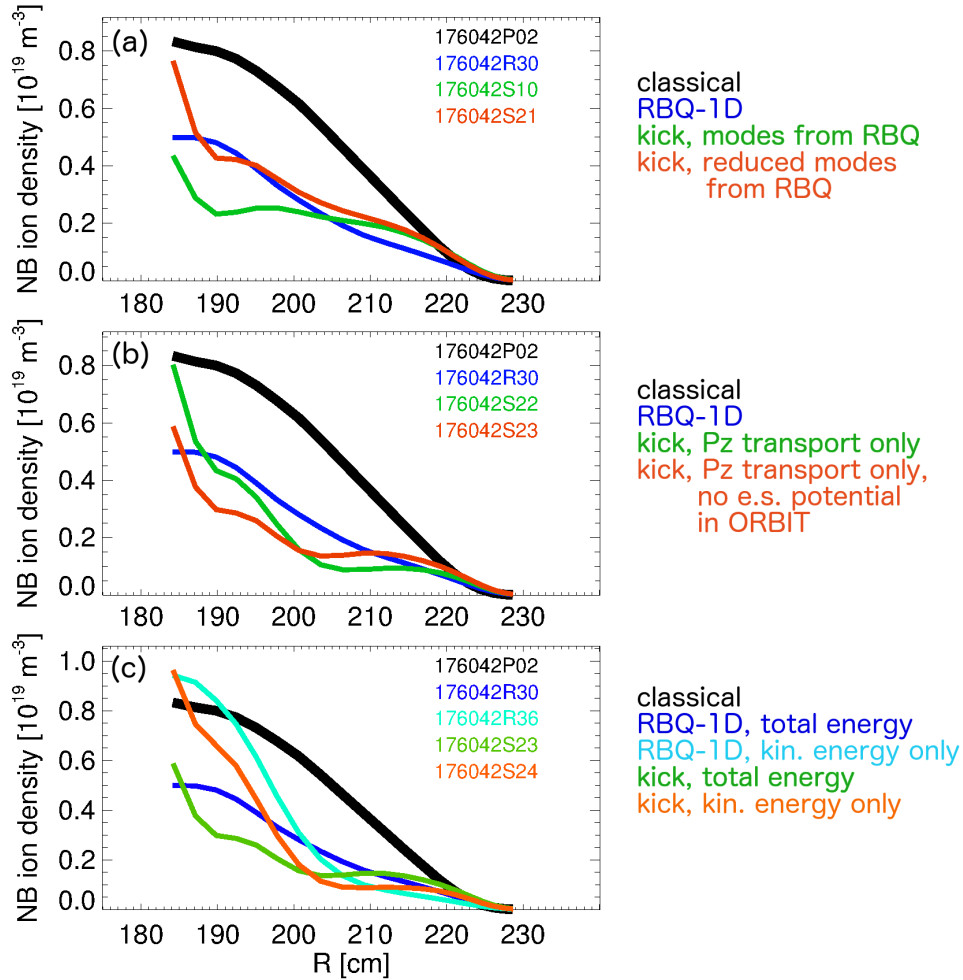


FIG. 40: Benchmark simulations between kick and RBQ-1D models. The kick model transport probability matrices are modified to mimic the main RBQ-1D assumptions in terms of number of harmonics retained in the model, transport in  $P_\zeta$  only and negligible electrostatic potential and rotation.

transport is forced to be diffusive as is done in RBQ-1D. This is done by replacing each  $p(\Delta P_\zeta)$  probability for the kick model with a gaussian fit function and compressing the probability at  $\Delta E = 0$ . Simulation results for this case are shown in Fig. 40b. NB ion density profiles maintain their core peaking, with some increase in the overall transport levels.

#### *Inclusion of finite electrostatic potential effects*

The last physics element considered here is the presence, in real discharges, of a finite radial electrostatic potential  $U_{pot}$ . The radial potential is related to the toroidal plasma velocity, with  $v_\phi \sim (-\nabla U_{pot} \times \mathbf{B}) \cdot \mathbf{e}_\phi$  (with  $\mathbf{e}_\phi$  the unity vector in the toroidal direction). For NB-heated plasmas with NB injection mostly in the co-current direction, common values for the electrostatic

potential on axis are  $U_{pot} \approx 10 - 20$  keV, which is comparable to the lower energy part of the NB ion distribution assuming typical NB injection energies of  $70 - 90$  keV. (Incidentally, electrostatic potential and plasma rotation were much lower for the ramp-up scenario (DIII-D #159243) for which good agreement was found between kick and RBQ-1D results).

There are several ways by which a finite  $U_{pot}$  can affect AE stability and fast ion transport calculations. The two main effects are:

1. A finite rotation associated with  $U_{pot} \neq 0$  affects the resonance condition, thus entering into the stability calculations and the estimates of resonance locations in the transport probabilities used by NUBEAM/TRANSP.
2. The proper constant of motion for the fast ion energy is the *total* energy, i.e. the sum of kinetic and potential energies. Since  $U_{pot} = U_{pot}(r)$ , kinetic energy is not conserved as fast ions travels across magnetic surfaces due to orbit drifts. If a finite  $U_{pot}$  is used in the simulations (as it typically is in TRANSP), neglecting the finite  $U_{pot}$  leads to inaccurate mapping of the fast ion energy onto the constant of motion variable.

Both (1) and (2) are taken into account in the kick model analysis. In RBQ-1D, (1) is properly taken into account in the resonant interaction calculations (e.g. to compute the mode drive) but it is not consistently treated by RBQ-1D itself, which uses the fast ion kinetic energy as main variable. Similarly for (2), RBQ-1D maps the transport probability matrices in terms of kinetic energy, rather than total energy.

Starting from the 'diffusive approximation' discussed above, kick model analysis has been repeated by artificially turning off the effects of a finite  $U_{pot}$  in ORBIT and in the way TRANSP/NUBEAM interpret the energy variable for the transport probabilities. Results are shown in Fig. 40c, which confirms that RBQ-1D and kick models show the same trends and qualitatively similar profiles as the effects of  $U_{pot} \neq 0$  are partially or completely neglected.

In summary, a detailed comparison of the results from kick and RBQ-1D models which takes into account their different physics assumptions shows that the two models reach a reasonable agreement once the same approximations are adopted. This benchmark result is a critical outcome from the JRT-18 modeling activities, since it suggests potential areas of improvement for the reduced models such as the extension to 2D transport in  $(E, P_\zeta)$  and a consistent treatment of the background electrostatic potential.

### Recommendations for future experimental and modeling activities

The following list contains suggestions on possible improvements to both experimental and modeling activities that emerged from the JRT-18 activities. Indeed, several difficulties were encountered over the year-long research that culminated in the present Report. *A-posteriori*, different approaches may have resulted in a even more fruitful study. The following suggestions aim to propose improvements to the approaches that were adopted for the JRT-18 work, so that future work can be even more effective.

- The JRT-18 experimental plan aimed at studying fast ion transport in steady-state high- $q_{min}$  discharges. This target proved to be quite challenging for the analysis of fast ion diagnostics such as FIDA and NPA, which struggle because of low signal-to-noise data at typical steady-state thermal plasma densities  $n_{e,i} \gtrsim 4 \times 10^{19} \text{ m}^{-3}$ . Measurements from Mirnov pickup coils had to be limited to an upper frequency of 500 kHz to cover the time window of interest ( $1000 \leq t \leq 5000 \text{ ms}$ ), resulting in insufficient over-sampling for the determination of toroidal mode numbers for modes with frequency near the Nyquist frequency,  $f \gtrsim 200 \text{ Khz}$ . The target toroidal field,  $B_0 \approx 1.7 \text{ T}$ , was at the lowest boundary for meaningful measurements through ECE. For future 'model validation' experiments, it is suggested to target plasma conditions that are more favorable for high signal-to-noise on fast ion diagnostics. Systems that are used for mode analysis, such as Mirnov coils and ECE, should also be optimized to provide the best available measurements of AE activity. Improvements of the available diagnostic tools, e.g. FIDA imaging and new NPA imaging systems on DIII-D, are expected to provide further constraints to validate EP transport models.
- The JRT-18 work has clearly indicated that accurate calculations of drive and damping rates for Alfénic modes are critical for predictions of mode stability and associated fast ion transport. To this end, improving present codes to include numerical distributions from codes such as TRANSP/NUBEAM for calculations of AE mode drive is required. Steps in this direction are being taken for NOVA-K.
- More extensive comparison between damping rate calculations from MHD codes with results from gyrokinetic simulation models is required.
- A validation of MHD/gyrokinetic codes against direct measurements of AE damping rates from active AE antennae is needed. At present, this activity can only be performed on JET.

- Validation of the reduced EP transport models needs to be extended to a larger set of experimental conditions. This requires more development work to make the models accessible to a broader set of users for production runs.

### Dissemination of the JRT-18 Results

#### *Presentations from JRT-18 related work*

- M. Podestà (PPPL), oral presentation at the 2018 IAEA-FEC Conference (Ahmedabad, India - October 2018), Reduced energetic particle transport models enable comprehensive time- dependent tokamak simulations. (A related Nuclear Fusion paper will be drafted in FY-18 for submission in early FY19).

- N. N. Gorelenkov (PPPL), invited talk at the 2018 APS-DPP Meeting (Portland, OR - November 2018), "Quasi-linear resonance broadened model for fast ion relaxation in the presence of Alfvénic instabilities"

- N. N. Gorelenkov (PPPL), "A quasi-linear resonance broadened model for fast ion relaxation in the presence of Alfvénic instabilities", Sherwood 2018

- N. N. Gorelenkov (PPPL), "A Quasi-linear model of fast ion relaxation due to Alfvénic instabilities", TTF 2018

- V. Aslanyan (MIT), "Progress in simulating Alfvén Eigenmodes on JET with the Gyrokinetic Toroidal Code (GTC)", TTF 2018

- W. W. Heidbrink (U.C. Irvine), "The phase-space dependence of fast-ion interaction with tearing modes", TTF 2018

- L. Bardoczi, (GA), "Test and Validation of TRANSP Kick-Model Predictive Capability of Neoclassical Tearing Mode Induced Fast Ion Transport in ITER Relevant DIII-D Plasmas", TTF 2018

- M. Podestà (PPPL), "Development of a reduced energetic particle transport model by fishbones for time-dependent integrated tokamak simulations", TTF 2018

- F. M. Poli (PPPL), "Optimization of ramp-up current evolution for improved access and sustainment of stable steady-state operation", TTF 2018

- F. M. Poli (PPPL), "How predict-first will change our approach to experimental planning", EPS 2018 (also reported by J. Ferron at the IOS-ITPA in spring 2018)

*Publications in FY-18, including papers from the 15th IAEA-TCM EP (Princeton, NJ Sept. 2017) with results from the FY-17 Notable complemented by initial JRT-18 results obtained during 1st and 2nd Quarters:*

- X. D. Du (GA), "Development and Verification of A Novel Scintillator-Based, Imaging Neutral Particle Analyzer in DIII-D Tokamak", Nucl. Fusion 58, 082006 (2018).

- N. N. Gorelenkov (PPPL), "Resonance line broadened quasilinear (RBQ) model for fast ion distribution relaxation due to Alfvénic eigenmodes", Nucl. Fusion 58, 082016 (2018).
- M. Podestà (PPPL), "Destabilization of counter-propagating Alfvénic instabilities by tangential, co-current neutral beam injection", Nucl. Fusion 58, 082023 (2018).
- W. W. Heidbrink (UC Irvine), "The interaction of fast ions with neoclassical tearing modes in different parts of phase space", Nucl. Fusion 58, 082027 (2018).
- V. Duarte (PPPL), "Study of the likelihood of Alfvénic mode bifurcation in NSTX and predictions for ITER baseline scenarios", Nucl. Fusion 58, 082018 (2018)
- G. Meng (PPPL), "Resonance frequency broadening of wave-particle interaction in tokamaks due to Alfvénic eigenmode", Nucl. Fusion 58, 082017 (2018).
- B. J. Q. Woods (U. York, UK), "Stochastic effects on phase-space holes and clumps in kinetic systems near marginal stability", Nucl. Fusion 58, 082015 (2018).
- D. Liu (UC Irvine), "Effect of sawtooth crashes on fast ion distribution in NSTX-U", Nucl. Fusion 58, 082028 (2018).
- D. Kim (PPPL), "ORBIT modeling of fast particle redistribution induced by sawtooth instability", Nucl. Fusion 58, 082029 (2018)

### Acknowledgements

The support of the NSTX-U and DIII-D Teams to run the experiments and provide the data required for this Report is gratefully acknowledged.

This material is based upon work supported by the US Department of Energy, Office of Science, Office of Fusion Energy Sciences under contracts number DE-AC02-09CH11466 and DE-FC02-04ER54698. NSTX-U at Princeton Plasma Physics Laboratory and DIII-D at General Atomics are DOE Office of Science User Facilities.

*Disclaimer:* This Report was prepared as an account of work sponsored by an agency of the United States Government. Neither the United States Government nor any agency thereof, nor any of their employees, makes any warranty, express or implied, or assumes any legal liability or responsibility for the accuracy, completeness, or usefulness of any information, apparatus, product, or process disclosed, or represents that its use would not infringe privately owned rights. Reference herein to any specific commercial product, process, or service by trade name, trademark, manufacturer, or otherwise, does not necessarily constitute or imply its endorsement, recommendation, or favoring by the United States Government or any agency thereof. The views and opinions of authors expressed herein do not necessarily state or reflect those of the United States Government or any agency thereof.

- 
- [1] M. Podestà, M. Gorelenkova, and R. B. White, *Plasma Phys. Control. Fusion* **56**, 055003 (2014).
- [2] M. Podestà, M. Gorelenkova, N. N. Gorelenkov, and R. B. White, *Plasma Phys. Control. Fusion* **59**, 095008 (2017).
- [3] N. N. Gorelenkov, V. N. Duarte, M. Podestà, and H. L. Berk, *Nucl. Fusion* **58**, 082016 (2018).
- [4] R. E. Waltz and E. M. Bass, *Nuclear Fusion* **54**, 104006 (2014).
- [5] R. E. Waltz, E. M. Bass, W. W. Heidbrink, and M. Van Zeeland, *Nucl. Fusion* **55**, 123012 (2015).
- [6] H. Sheng, R. E. Waltz, and G. M. Staebler, *Phys. Plasmas* **24**, 072305 (2017).
- [7] W. W. Heidbrink, C. Collins, M. Podestà, G. J. Kramer, D. Pace, C. Petty, L. Stagner, M. Van Zeeland, R. B. White, and Y. Zhu, *Phys. Plasmas* **24**, 056109 (2017).
- [8] M. A. Van Zeeland, G. J. Kramer, M. E. Austin, R. L. Boivin, W. W. Heidbrink, M. A. Makowski, G. R. McKee, R. Nazikian, W. M. Solomon, and G. Wang, *Phys. Rev. Lett.* **97**, 135001 (2006).
- [9] W. W. Heidbrink, D. Liu, Y. Luo, E. Ruskov, and B. Geiger, *Commun. Comput. Phys.* **10**, 716 (2011).
- [10] V. N. Duarte, H. Berk, N. N. Gorelenkov, W. W. Heidbrink, G. J. Kramer, R. Nazikian, D. Pace, M. Podestà, B. Tobias, and M. A. Van Zeeland, *Nucl. Fusion* **57**, 054001 (2017).
- [11] V. N. Duarte, N. N. Gorelenkov, M. Schneller, E. D. Fredrickson, M. Podestà, and H. L. Berk, *Nucl. Fusion* **58**, 082018 (2018).
- [12] M. Podestà, R. E. Bell, N. A. Crocker, E. D. Fredrickson, N. N. Gorelenkov, W. W. Heidbrink, S. Kubota, B. P. LeBlanc, and H. Yuh, *Nucl. Fusion* **51**, 063035 (2011).
- [13] M. Podestà, R. E. Bell, A. Bortolon, N. A. Crocker, D. S. Darrow, A. Diallo, E. D. Fredrickson, G. Fu, N. N. Gorelenkov, W. W. Heidbrink, G. J. Kramer, S. Kubota, B. P. LeBlanc, S. S. Medley, and H. Yuh, *Nucl. Fusion* **52**, 094001 (2012).
- [14] S. Kubota, W. A. Peebles, X. V. Nguyen, N. A. Crocker, and A. L. Roquemore, *Rev. Sci. Instr.* **77**, 10E926 (2006).
- [15] N. A. Crocker, W. A. Peebles, S. Kubota, J. Zhang, R. E. Bell, E. D. Fredrickson, N. N. Gorelenkov, B. P. LeBlanc, J. E. Menard, M. Podestà, S. A. Sabbagh, K. Tritz, and H. Yuh, *Plasma Phys. Control. Fusion* **53**, 105001 (2011).
- [16] E. M. Bass and R. E. Waltz, in *US/EU TTF Workshop* (San Diego, CA - USA, 2018).
- [17] R. J. Hawryluk, in *Physics of Plasmas Close to Thermonuclear Conditions* (CEC, Brussels, 1980).
- [18] R. J. Goldston, D. C. McCune, H. H. Towner, S. L. Davis, R. J. Hawryluk, and G. L. Schmidt, *J. Comput. Phys.* **43**, 61 (1981).
- [19] For more details on the TRANSP code, please refer to the TRANSP webpage at <http://w3.pppl.gov/~pshare/help/transp.htm>.
- [20] A. Pankin, D. McCune, R. Andre, G. Bateman, and A. Kritz, *Computer Physics Communication* **159**, 157 (2004).
- [21] B. J. Q. Woods, V. N. Duarte, A. J. De-Gol, N. N. Gorelenkov, and R. G. L. Vann, *Nucl. Fusion* **58**,

- 082015 (2018).
- [22] W. E. Drummond and D. Pines, Nucl. Fusion, Suppl. Pt. 3 , 1049 (1962).
- [23] A. A. Vedenov, E. P. Velikhov, and R. Z. Sagdeev, Sov. Phys. Usp. , 332 (1961).
- [24] H. L. Berk, B. N. Breizman, J. Fitzpatrick, M. S. Pekker, H. V. Wong, and K. L. Wong, Phys. Plasmas **3**, 1827 (1996).
- [25] K. Ghanous, N. N. Gorelenkov, H. L. Berk, W. W. Heidbrink, and M. A. Van Zeeland, Phys. Plasmas **19**, 092511 (2012).
- [26] N. N. Gorelenkov and V. N. Duarte, Phys. Plasmas (submitted, 2018).
- [27] G. Meng, N. N. Gorelenkov, V. N. Duarte, H. L. Berk, R. B. White, and X. G. Wang, Nucl. Fusion **58**, 082017 (2018).
- [28] R. B. White, N. N. Gorelenkov, V. N. Duarte, and H. L. Berk, Phys. Plasmas (submitted, 2018).
- [29] M. Podestà, E. D. Fredrickson, and M. Gorelenkova, Nucl. Fusion **58**, 082023 (2018).
- [30] in IAEA Fusion Energy Conference (Ahmedabad, India, 2018).
- [31] W. W. Heidbrink, L. Bardóczi, C. S. Collins, G. J. Kramer, D. J. Lin, C. M. Muscatello, M. Podestà, L. Stagner, M. A. Van Zeeland, , and Y. B. Zhu, in 15th IAEA-TM EP meeting (Princeton, NJ - USA, 2017).
- [32] L. Bardóczi, M. Podestà, W. Heidbrink, and M. A. Van Zeeland, in US/EU TTF Workshop (San Diego, CA - USA, 2018).
- [33] W. W. Heidbrink, L. Bardóczi, C. S. Collins, G. J. Kramer, R. J. La Haye, D. J. Lin, C. M. Muscatello, M. Podestà, L. Stagner, M. A. Van Zeeland, and Y. B. Zhu, in US/EU TTF Workshop (San Diego, CA - USA, 2018).
- [34] W. W. Heidbrink, L. Bardóczi, C. S. Collins, G. J. Kramer, D. J. Lin, C. M. Muscatello, M. Podestà, L. Stagner, M. A. Van Zeeland, , and Y. B. Zhu, Nucl. Fusion **58**, 082027 (2018).
- [35] L. Bardóczi, M. Podestà, W. W. Heidbrink, and M. A. Van Zeeland, Plasma Phys. Control. Fusion (submitted, 2018).
- [36] M. Podestà, in US/EU TTF Workshop (San Diego, CA - USA, 2018).
- [37] D. Liu, W. W. Heidbrink, M. Podestà, G. Z. Hao, D. S. Darrow, E. D. Fredrickson, and D. Kim, Nucl. Fusion **58**, 082028 (2018).
- [38] D. Kim, M. Podestà, D. Liu, and F. M. Poli, Nucl. Fusion **58**, 082029 (2018).
- [39] R. B. White and M. S. Chance, Phys. Fluids **27**, 2455 (1984).
- [40] J. Candy and R. E. Waltz, J. Comp. Phys. **186**, 545 (2003).
- [41] Z. Lin, T. S. Hahm, W. W. Lee, W. M. Tang, and R. B. White, Science **281**, 1835 (1998).
- [42] V. Aslanyan, M. Porkolab, S. Taimourzadeh, L. Shi, Z. Lin, G. Dong, P. Puglia, S. E. Sharapov, J. Mailloux, M. Tsalas, M. Maslov, A. Whitehead, R. Scannell, S. Gerasimov, S. Dorling, S. Dowson, H. K. Sheikh, T. Blackman, G. Jones, A. Goodyear, K. K. Kirov, R. Dumont, P. Blanchard, A. Fasoli, D. Testa, and JET Contributors, in US/EU TTF 2018 Workshop (San Diego, CA - USA, 2018).
- [43] J. Snipes, N. N. Gorelenkov, and J. A. Sears, Nucl. Fusion **46**, 1036 (2006).

- [44] J. A. Sears, R. R. Parker, and J. Snipes, *Nucl. Fusion* **52**, 083003 (2012).
- [45] F. Nabais, V. Aslanyan, D. Borba, R. Coelho, R. Dumont, J. Ferreira, A. Figueiredo, M. Fitzgerald, E. Lerche, J. Mailloux, M. Mantsinen, P. Rodrigues, M. Porkolab, P. Puglia, S. Sharapov, and JET Contributors, *Nucl. Fusion* **58**, 082007 (2018).
- [46] Y. Kazakov, J. Ongena, J. Wright, S. Wukitch, E. Lerche, M. Mantsinen, D. Van Eester, T. Craciunescu, V. Kiptily, Y. Lin, M. Nocente, F. Nabais, M. Nave, Y. Baranov, J. Bielecki, R. Bilato, V. Bobkov, K. Crombe, A. Czarnecka, and M. Koppén, *Nat. Phys.* **13**, 973 (2017).
- [47] S. Taimourzadeh, E. M. Bass, Y. Chen, C. S. Collins, N. N. Gorelenkov, W. W. Heidbrink, A. Koenies, Z. Lin, Z. X. Lu, D. A. Spong, Y. Todo, R. E. Waltz, G. Yu, M. E. Austin, A. Mishchenko, L. Shi, J. Varela, and Y. Zhu, in preparation (2018).
- [48] X. D. Du, M. A. Van Zeeland, W. W. Heidbrink, and D. Su, *Nucl. Fusion* **58**, 082006 (2018).
- [49] <https://d3denergetic.github.io/FIDASIM/>.
- [50] L. Stagner and W. W. Heidbrink, *Phys. Plasmas* **24**, 092505 (2017).
- [51] N. C. Logan, B. A. Grierson, S. R. Haskey, S. P. Smith, O. Meneghini, and D. Eldon, *Fusion science and technology* **74**, 125 (2018).
- [52] C. S. Collins, W. W. Heidbrink, M. Podestà, R. B. White, G. J. Kramer, D. C. Pace, C. C. Petty, L. Stagner, M. A. VanZeeland, Y. B. Zhu, and the DIII-D team, *Nucl. Fusion* **57**, 086005 (2017).
- [53] F. Poli, D. Boyer, B. Grierson, W. Guttenfelder, G. J. Kramer, N. Logan, M. Podestà, Z. Wang, K. Thome, B. Victor, J. Ferron, and C. Holcomb, in US/EU TTF Workshop (San Diego, CA - USA, 2018).
- [54] F. Poli, B. Grierson, M. Podestà, Z. Wang, J. Ferron, C. Holcomb, B. Victor, and K. Thome, in 45th EPS Conference on Plasma Physics (Prague, Czech Republic, 2018).
- [55] P. B. Snyder, R. J. Groebner, J. W. Hughes, T. H. Osborne, M. Beurskens, A. W. Leonard, H. R. Wilson, and X. Q. Xu, *Nucl. Fusion* **51**, 103016 (2011).
- [56] C. T. Holcomb, W. W. Heidbrink, J. R. Ferron, M. A. Van Zeeland, A. M. Garofalo, W. M. Solomon, X. Gong, D. Mueller, B. Grierson, E. M. Bass, C. S. Collins, J. M. Park, K. Kim, T. C. Luce, F. Turco, D. C. Pace, Q. Ren, and M. Podestà, *Phys. Plasmas* **22**, 055904 (2015).
- [57] C. S. Collins, W. W. Heidbrink, M. E. Austin, G. J. Kramer, D. C. Pace, C. C. Petty, L. Stagner, M. A. Van Zeeland, R. B. White, Y. B. Zhu, and DIII-D team, *Phys. Rev. Letters* **116**, 095001 (2016).
- [58] C. Collins, C. Holcomb, M. Van Zeeland, J. R. Ferron, C. C. Petty, D. Shiraki, M. Podestà, W. W. Heidbrink, X. Du, G. J. Kramer, N. Gorelenkov, F. Poli, and B. Grierson, “Reduce AE induced EP transport in high-qmin steady state scenarios using AE control tools,” DIII-D Mini-Proposal no. 2018-13-02.
- [59] B. S. Victor, K. E. Thome, J. R. Ferron, C. T. Holcomb, F. M. Poli, E. Schuster, W. Wehner, J. M. Park, B. A. Grierson, C. C. Petty, N. I. Eidietis, J. Lohr, and R. I. Pinsker, “Using predictive modeling and feedback control to achieve stable, stationary high-qmin operations,” DIII-D Mini-Proposal no. 2018-22-01.

- [60] M. Weiland, R. Bilato, R. Dux, B. Geiger, A. Lebschy, F. Felici, R. Fischer, D. Rittich, M. Van Zeeland, and the ASDEX Upgrade Team and the Eurofusion MST1 Team, *Nucl. Fusion* **58**, 082032 (2018).
- [61] C. T. Holcomb, J. R. Ferron, T. C. Luce, J. C. DeBoo, J. M. Park, A. E. White, F. Turco, T. L. Rhodes, E. J. Doyle, L. Schmitz, M. A. Van Zeeland, and G. R. McKee, *Phys. Plasmas* **19**, 032501 (2012).
- [62] W. W. Heidbrink, J. R. Ferron, C. T. Holcomb, M. A. Van Zeeland, X. Chen, C. M. Collins, A. Garofalo, X. Gong, B. A. Grierson, M. Podestà, L. Stagner, and Y. Zhu, *Plasma Phys. Control. Fusion* **56**, 095030 (2014).
- [63] W. W. Heidbrink, L. Bardóczi, C. S. Collins, G. J. Kramer, R. J. La Haye, D. J. Lin, C. M. Muscatello, M. Podestà, L. Stagner, M. A. Van Zeeland, and Y. B. Zhu, *Nucl. Fusion* **58**, 082027 (2018).
- [64] W. W. Heidbrink, C. Collins, L. Stagner, Y. B. Zhu, C. C. Petty, and M. Van Zeeland, *Nucl. Fusion* **56**, 112011 (2016).
- [65] R. B. White, N. N. Gorelenkov, W. W. Heidbrink, and M. A. V. Zeeland, *Plasma Phys. Control. Fusion* **52**, 045012 (2010).
- [66] These activities have been coordinated with F. M. Poli and other personnel of the ITER and Tokamak Department (PPPL) working on the FY-18 Milestone: "Predictive modeling activities in support of high q-min experiments with reduced MHD and Alfvénic instabilities on DIII-D".
- [67] Most of the work described in the following paragraphs of this Section was conducted during the second quarter of FY-18, cf. JRT-18 Second Quarter Report. A short description of the activities and the main conclusions are summarized here for completeness.